AFRL-AFOSR-VA-TR-2019-0172

Multifunctional Organic-Inorganic Nanocomposites with Unprecedented Control Over Dimensions, Compositions and Architectures as well as Tailored Properties

Zhiqun Lin
GEORGIA TECH RESEARCH CORPORATION

05/24/2019
Final Report

Air Force Research Laboratory
AF Office Of Scientific Research (AFOSR)/ RTB2
Arlington, Virginia 22203
Air Force Materiel Command

DISTRIBUTION A: Distribution approved for public release.

REPORT DOCUMENTATION PAGE

Form Approved
OMB No. 0704-0188

1. REPORT DATE *(DD-MM-YYYY)*	2. REPORT TYPE	3. DATES COVERED *(From - To)*
19-06-2019	Final Performance	01 May 2016 to 30 Apr 2019

4. TITLE AND SUBTITLE
Multifunctional Organic-Inorganic Nanocomposites with Unprecedented Control Over Dimensions, Compositions and Architectures as well as Tailored Properties

5a. CONTRACT NUMBER

5b. GRANT NUMBER
FA9550-16-1-0187

5c. PROGRAM ELEMENT NUMBER
61102F

6. AUTHOR(S)
Zhiqun Lin

5d. PROJECT NUMBER

5e. TASK NUMBER

5f. WORK UNIT NUMBER

7. PERFORMING ORGANIZATION NAME(S) AND ADDRESS(ES)
GEORGIA TECH RESEARCH CORPORATION
505 10TH ST NW
ATLANTA, GA 30318-5775 US

8. PERFORMING ORGANIZATION REPORT NUMBER

9. SPONSORING/MONITORING AGENCY NAME(S) AND ADDRESS(ES)
AF Office of Scientific Research
875 N. Randolph St. Room 3112
Arlington, VA 22203

10. SPONSOR/MONITOR'S ACRONYM(S)
AFRL/AFOSR RTB2

11. SPONSOR/MONITOR'S REPORT NUMBER(S)
AFRL-AFOSR-VA-TR-2019-0172

12. DISTRIBUTION/AVAILABILITY STATEMENT
A DISTRIBUTION UNLIMITED: PB Public Release

13. SUPPLEMENTARY NOTES

14. ABSTRACT
Over the past year, we have developed several robust strategies for crafting stable hairy nanoparticles (NPs). First, we report in-situ crafting of noble metal NPs (i.e., Au) intimately and permanently ligated by thermoresponsive polymers (i.e., poly (Nisopropylacrylamide);
PNIPAM) using double-hydrophilic star-like block copolymer as nanoreactor to resolve the paradox noted above. The strongly ligated PNIPAM on the Au NP surface effectively eliminate the inevitable ligand dissociation issue due to the dynamic binding nature of ligands as in copious past work. As such, two seemingly contradictory observations on both temperature-dependent optical and catalytic properties largely encountered in the literature are elucidated by capitalizing on judiciously designed thermoresponsive PNIPAM-capped Au NP system. Intriguingly, as temperature increases over the lower critical solution temperature (LCST) of PNIPAM, plasmonic absorption peak of PNIPAM-capped Au NPs redshifts accompanied by an increase in intensity in the absence of free linear PNIPAM, whereas the characteristic absorption peak red-shifts greatly with a decreased intensity in the presence of deliberately introduced linear PNIPAM. Moreover, remarkably, the absence or addition of free linear PNIPAM also accounts for a non-monotonic (i.e., non-Arrhenius) or a switchable 'on/off' catalytic performance of PNIPAM-capped Au NPs, respectively. The star-like block copolymer nanoreactor strategy is robust and enables the convenient creation of a rich diversity of new hybrid materials composed of functional NPs (e.g., Ag, TiO2, SiO2, Fe3O4, and BaTiO3) permanently tethered with polymers of interest, thereby underpinning future advances in optics, optoelectronics, catalysis, medical imaging and therapy, nanotechnology, and biotechnology. Second, we also demonstrated a general amphiphilic star-like block copolymer nanoreactor

15. SUBJECT TERMS
block copolymer, nanoparticle synthesis, core shell nanoparticles, organic nano reactors

16. SECURITY CLASSIFICATION OF:			17. LIMITATION OF ABSTRACT	18. NUMBER OF PAGES	19a. NAME OF RESPONSIBLE PERSON
a. REPORT	b. ABSTRACT	c. THIS PAGE			CASTER, KENNETH
Unclassified	Unclassified	Unclassified	UU		19b. TELEPHONE NUMBER *(Include area code)* 703-588-8487

Multifunctional Organic-Inorganic Nanocomposites with Unprecedented Control Over Dimensions, Compositions and Architectures

Zhiqun Lin; Professor
School of Materials Science and Engineering, Georgia Institute of Technology,
Atlanta, GA 30332

Final Report on the AFOSR project: FA9550-16-1-0187 **(05/01/2018-04/30/2019)**

Over the past year, we have made very good progress on the project. 11 papers have been published under this support. The key results are summarized as follows.

Part A: Optical and Catalytic Activities in Thermoresponsive Nanoparticles via Permanent-Ligating with Temperature-Sensitive Polymers

Science Advances (submitted)

Stimuli-responsive nanoparticles (NPs) exhibit an exciting variety of physical properties that depend sensitively on the stimuli triggered (e.g., solvent polarity, ionic strength, light, pH, temperature, magnetic field, etc.). Among various stimuli-responsive NPs developed, thermoresponsive NPs composed of thermally responsive polymers capped on the surface of functional NPs of interest stand out as a particularly interesting class of organic-inorganic hybrid nanomaterials. They render convenient tailoring of the plasmonic, magnetic, semiconducting, catalytic properties by simply regulating temperature for use in controlled delivery, catalysis, molecule detection, and biological science.[1,2] Poly(*N*-isopropylacrylamide) (PNIPAM) is a widely studied thermoresponsive polymer that undergoes a phase transition from water-swollen state to globular state when heating its aqueous solution above the lower critical solution temperature (LCST, ~32°C) of PNIPAM.[3] Among several impressive routes to PNIPAM-capped NPs (e.g., Au and Fe_3O_4) emerged, grafting-from/grafting-to approach represents the most commonly used technique.[4-6] However, this approach requires a high selectivity between the inorganic NP core and the functional end-groups in grafted molecules (i.e., polar groups for metal NP core and polar charged groups for metal oxide NP core).[7,8] Consequently, the tedious synthetic procedures are often invoked.[9] Moreover, it is also notable that the PNIPAM ligands tethered on the NP surface via a grafting-from or grafting-to approach often experience a dynamic binding characteristic due to non-covalent interaction between PNIPAM and NP.[4-6] Consequently, PNIPAM may dissociate from the NP surface after a long period of time or deteriorate when the experimental condition changes (e.g., detached during purification,[10] and breakage of semi-covalent Au-thiol-end-functionalized PNIPAM (Au-SH) binding in PNIPAM-capped Au NPs at temperature above 60°C[11,12]), thereby significantly affecting the thermoresponsive capability of the system.

It is important to note that linear block copolymer micelle has recently been used to template the synthesis of PNIPAM-capped Au NPs.[13] However, this approach is limited in scope as the shape of spherical micelles is dynamically stable and thus difficult to be maintained.[14] A variation in solution concentration, solvent, temperature, and pH would lead

to the formation of NPs with non-uniform size and shape along with the presence of free linear block copolymer resulted from the dissociation of micelles.[15,16] Obviously, it remains challenging to produce highly stable uniform thermoresponsive NPs for exploring their size- and shape-dependent physical properties.

Despite the apparent similarity in either synthetic routes to NPs or size and shape of the resulting NPs, the reported PNIPAM-capped Au NPs often encounter two disparate thermoresponsive behaviors upon heating above the phase transition temperature (i.e., LCST) of PNIPAM,[17] that is, the occurrence of shrinkage of the PNIPAM shell without the aggregation of NPs in some literature[4,18,19] (i.e., small-sized) while the formation of the aggregated NPs in the other literature[6,20,21] (i.e., comparatively large-sized). Accordingly, such disparity has led to the observation of two markedly different optical properties as well as catalytic activities for the PNIPAM-capped Au NP system, representing in small red-shift with the increased intensity[18] *versus* large red-shift of plasmonic absorption with the decreased intensity[20] (i.e., optical properties), and a non-monotonic[19] *versus* a distinct "on/off"[21] catalytic performance of Au NPs, as temperature rises over LCST. However, no effort has been concentrated on resolving these discrepancies plagued in the PNIPAM-capped Au NP system.[17] Clearly, it is highly desirable to identify the explicit reason that is responsible for these contradictory conclusions due to both fundamental and practical importance.

Herein, we develop a robust nanoreactor strategy for *in-situ* crafting monodisperse stably-ligated thermoresponsive noble metal NPs with the aim of reconciling the paradoxical observations noted above. Central to this strategy is the judicious design of double-hydrophilic unimolecular star-like poly(acrylic acid)-*block*-poly(*N*-isopropylacrylamide) (denoted PAA-*b*-PNIPAM) diblock copolymer as nanoreactor to yield Au NPs *intimately* and *permanently* ligated by thermoresponsive PNIPAM. A set of star-like PAA-*b*-PNIPAM diblock copolymers with well-defined yet tunable molecular weights (MWs) and low polydispersity index (PDI) are first synthesized via sequential atom transfer radical polymerization (ATRP) of *tert*-butyl acrylate (*t*BA) and *N*-isopropylacrylamide (NIPAM) monomers, respectively, from a *β*-cyclodextrin (*β*-CD)-based macroinitiator (i.e., forming amphiphilic star-like poly(*tert*-butyl acrylate)-*block*-poly(*N*-isopropylacrylamide); P*t*BA-*b*-PNIPAM), followed by hydrolysis of inner hydrophobic P*t*BA into hydrophilic PAA. Compared to linear block copolymer micelle counterpart which is only dynamically stable, the resulting double-hydrophilic star-like PAA-*b*-PNIPAM forms monodisperse, statically stable spherical unimolecular micelle (i.e., comprising a single copolymer macromolecule).[14,22] Subsequently, star-like PAA-*b*-PNIPAM is exploited as nanoreactor to craft PNIPAM-capped Au NPs. Notably, strong coordination between carboxylic acid groups of inner PAA chains and the metal moieties of Au precursors in conjunction with the stable, spherical structure of unimolecular micelle render the preferential partition of abundant precursors in the compartment occupied by PAA chains,[23,24] leading to *in-situ* formation of PNIPAM-capped Au NPs. Importantly, the surface of Au NP is *intimately* and *permanently* ligated by PNIPAM as a result of original covalent bonding between outer PNIPAM and PAA blocks in star-like PAA-*b*-PNIPAM. Quite intriguingly,

these PNIPAM-capped Au NPs remain dispersed when heating the NP aqueous solution over LCST of PNIPAM. Accordingly, PNIPAM-capped Au NPs exhibit a red-shift of plasmonic absorption peak with increased intensity (i.e., optical property) and a non-monotonic (i.e., non-Arrhenius) catalytic activity. In stark contrast, the addition of free linear PNIPAM chains into PNIPAM-capped Au NP aqueous solution is found to trigger the aggregation of NPs with the extent of aggregation relying on the amount of the added linear PNIPAM, as temperature increases over LCST. Consequently, a comparatively larger red-shift of plasmonic absorption peak with decreased intensity and a distinct "on/off" catalysis of PNIPAM-capped Au NPs are observed. The catalytic activity is scrutinized using the model catalytic reaction of 4-nitrophenol (4-NP) to 4-aminophenol (4-AP) reduced by sodium borohydride ($NaBH_4$).

These studies lead us to conclude that the contradictory phenomena reported in the literature described above may be ascribed to the quality of thermoresponsive polymer passivation on the surface of NP. When PNIPAM ligands are not strongly attached to the Au NP surface,[6,20,21] the partial dissociation of PNIPAM into the solution occurs and thus becomes free linear PNIPAM chains. They function as the physical crosslinkers to facilitate the aggregation of Au NPs when temperature increases above LCST, and correspondingly a red-shift of plasmonic absorption with decreased intensity and an "on/off" catalytic behavior are observed. Contrastively, with a strong tethering of PNIPAM ligands on the Au NP surface[4,18,19] and the temperature rising over LCST, only the collapse (i.e., shrinkage) of surface PNIPAM ligands occurred and thus no aggregation of Au NPs is resulted in, and hence a smaller red-shift of plasmonic absorption with increased intensity and a non-monotonic catalytic action are yielded.

It is also noteworthy that our star-like block copolymer nanoreactor strategy is general, providing a robust platform for synthesis of virtually unlimited thermoresponsive polymer-capped functional NPs, for example, plasmonic Ag, semiconducting TiO_2, magnetic Fe_3O_4, and ferroelectric $BaTiO_3$.

Results and Discussion

It is important to note that, in contrast to the aforementioned conventional methods (e.g., grafting-from/grafting-to, etc.), our star-like block copolymer nanoreactor strategy offers several peculiar advantages. *First*, as ATRP is a living free radical polymerization technique,[25] it renders the synthesis of unimolecular star-like diblock copolymer with well-defined MW and low PDI of each block. Thus, by controlling the ATRP time of *t*BA and NIPAM monomers, the MWs (i.e., lengths) of the resulting PAA and PNIPAM blocks can be readily tuned, which in turn yields PNIPAM-capped Au NPs with monodisperse yet tailorable diameter of Au NPs and length of PNIPAM. *Second*, the covalently-linked PAA-*b*-PNIPAM in star-like diblock copolymer ensures the crafting of Au NPs with *intimate* and *permanent* ligating of PNIPAM as the growth of Au NPs is templated by PAA blocks, thereby eliminating the possible PNIPAM ligand dissociation issue as encountered in the past work,[5,6,10,11] and thus enabling the credible study of thermally-responsive optical and catalytic properties of PNIPAM-capped Au NPs. *Third*, the star-like block copolymer strategy can be

conveniently extended to craft various PNIPAM-capped or other stimuli-responsive polymer-capped plasmonic (e.g., Ag), semiconducting (e.g., TiO_2), insulating (e.g., SiO_2), magnetic (e.g., Fe_3O_4), and ferroelectric (e.g., $BaTiO_3$) NPs, thereby providing a platform for creating smart organic-inorganic hybrid nanomaterials and systems for fundamental studies on their stimuli-dependent physical properties as well as various technological applications.

We note that the two contradictory observations upon heating over the LCST of PNIPAM, that is, *aggregated* as opposed to *dispersed* NPs as well as the corresponding different physical properties in the PNIPAM-capped NP systems (e.g., Au, Fe_3O_4, Co) reported in the literature involved the NPs mostly prepared by either grafting-from or grafting-to methods,[17] from which the grafted PNIPAM chains were usually not stable on the surface of NPs.[5,6,10,11] Interestingly, for the PNIPAM-capped Au NP system with a crosslinked PNIPAM shell, the collapsed PNIPAM without aggregation was found upon heating.[4,18] On the basis of these evidences, it is conceivable that linear PNIPAM chains detached from the NP surface may exist in the NP aqueous solution.[10,11] These free linear PNIPAM chains may be responsible for the seemingly opposite results observed. In sharp contrast, our star-like block copolymer nanoreactor strategy employed to craft Au NPs *strongly* and *permanently* ligated by PNIPAM chains, thereby effectively circumventing the creation of any detached linear PNIPAM chains.

Figure 1a depicts our synthetic strategy for crafting PNIPAM-capped Au NP by capitalizing on unimolecular double-hydrophilic star-like PAA-*b*-PNIPAM diblock copolymer as nanoreactor. Briefly, 21-Br-β-CD (upper left panel in **Figure 1a**) was firstly prepared by thoroughly esterifying 21 hydroxyl groups on β-CD. Using 21-Br-β-CD as the macroinitiator, a series of amphiphilic unimolecular star-like P*t*BA-*b*-PNIPAM diblock copolymers were synthesized via sequential ATRP of *t*BA and NIPAM monomers. The living characteristic of ATRP[25] affords the synthesis of star-like polymers (i.e., star-like P*t*BA, upper central panel; and star-like P*t*BA-*b*-PNIPAM, upper right panel in **Figure 1a**) with well-defined yet tunable MW and narrow MW distribution of each block. Subsequently, the inner hydrophobic P*t*BA blocks were then hydrolyzed into hydrophilic PAA using trifluoroacetic acid (TFA), yielding star-like PAA-*b*-PNIPAM (lower right panel in **Figure 1a**). The successful synthesis of star-like P*t*BA, star-like P*t*BA-*b*-PNIPAM and star-like PAA-*b*-PNIPAM was verified by proton NMR (^{1}H NMR).

Subsequently, as-synthesized star-like PAA-*b*-PNIPAM copolymers were exploited as nanoreactors to direct the *in-situ* crafting of PNIPAM-capped Au NPs (lower panels in **Figure 1a)**. The reaction was performed in the mixed solvents of DMF/DPE at a volume ratio of 8/2. As DMF is a good solvent for both PAA and PNIPAM, and DPE is a good solvent only for PAA while a poor solvent for PNIPAM, structurally stable unimolecular micelles with spherical shape composed of the expanded inner PAA chains and the collapsed outer PNIPAM chains were resulted in. When the Au precursors were introduced into the solution, the strong coordination interaction between the carboxylic acid groups (-COOH) of the inner PAA blocks in star-like PAA-*b*-PNIPAM and the metal moieties of precursors in conjunction with the stable, spherical structure of unimolecular micelle led to the preferential partitioning

of the precursors in the compartment occupied by PAA chains (lower central panel in **Figure 1a**), and eventually the formation of PNIPAM-capped Au NP (lower left panel in **Figure 1a**).

As mentioned above, the outer PNIPAM and the inner PAA blocks are originally covalently linked, thus the Au NP surface is *intimately* and *permanently* ligated by hydrophilic, thermoresponsive PNIPAM chains, thereby not only imparting their good dispersion in polar solvents (e.g., water at room temperature) but also eliminating the potential detachment of PNIPAM ligands from the Au NP surface (i.e., ensuring the absence of free PNIPAM chains created in the system). It is also important to note that any linear polymers formed during star-like polymer synthesis can be completely removed by fractional precipitation.[26,27] By rationally designing the MW (i.e., length) of PAA and PNIPAM blocks in star-like diblock copolymer via tuning the ATRP time of P*t*BA and PNIPAM, the diameter of Au NP and the length of PNIPAM ligands can be tailored, respectively.

The *in-situ* formation of PNIPAM-capped Au NPs using star-like PAA-*b*-PNIPAM as nanoreactor was monitored by tracking the absorption spectra of the reaction solutions after adding the reducer. As the reaction time increased, the SPR peak intensity increased with the decreased full-width-at-half-maximum (FWHM). **Figure 1b-d** shows the representative transmission electron microscope (TEM) images of PNIPAM-capped Au NPs. As-synthesized Au NPs are monodisperse with an average diameter of 14.5 nm ± 0.3 nm (**Figure 1b**). A representative high-resolution TEM (HRTEM) image of a single PNIPAM-capped Au NP clearly shows the crystalline structure with a lattice spacing of 0.239 nm, which agrees well with the (111) interplanar distance of the fcc Au. Notably, the volume ratio of the mixed solvents (i.e., DMF to DPE) played an important role in creating monodisperse PNIPAM-capped Au NPs. At volume ratio of V_{DMF}/V_{DPE} of 10:0 and 6:4, relatively irregular Au NPs were observed, while monodisperse Au NPs were seen at V_{DMF}/V_{DPE} of 8:2 (i.e., DMF/DPE = 8/2 in **Figure 1b-d**), which can be understood by considering the change of chain conformation of PAA and PNIPAM blocks in the mixed solvents of varied volume ratios. Unless otherwise specified, PNIPAM-capped Au NPs discussed below were crafted at V_{DMF}/V_{DPE} of 8:2 (**Figures 1-5**). To visualize the PNIPAM ligands situated on the Au NP surface, the TEM sample was treated with phosphotungstic acid to preferentially stain PNIPAM.[28] The PNIPAM ligands formed a layer of shell with a thickness of approximately 10.6 nm ± 0.5 nm at 25 °C, as clearly evidenced in **Figure 1c**. Thermogravimetric analysis measurement revealed the weight fraction of the Au NP was 76.8%. When the temperature was raised above the LCST, the PNIPAM ligands collapsed with a decreased thickness of approximately 5.8 nm ± 0.2 nm (**Figure 1d**).

The thermoresponsiveness of PNIPAM-capped Au NPs was then studied by dynamic light scattering (DLS), where the change of hydrodynamic diameter (D_h) of PNIPAM-capped Au NPs can be seen as the temperature increased from 10°C to 50°C. An obvious volume change of the ligated PNIPAM chains around 32°C was seen. Notably, the similar LCST of the PNIPAM ligands to the bulk PNIPAM[3] revealed that the presence of Au NP does not greatly affect the thermoresponsiveness of PNIPAM chains that shell its surface. The size of PNIPAM-capped Au NPs determined by DLS is larger than that by TEM (**Figure 1b-d**) at

25°C, which can be ascribed to the two kinds of water surrounding PNIPAM. One is the bound water to hydrophilic domains (i.e., N, O atoms) of PNIPAM via hydrogen bonding and the other is water molecules around the hydrophobic isopropyl groups of PNIPAM (i.e., forming the so-called "water cages" or "water clathrates").[29] When the temperature is above the LCST of PNIPAM (e.g., 50°C), the water cages are dissociated from the isopropyl groups while the bound water may likely partially retain around the hydrophilic domains due to the strong hydrogen bonding between them,[4,29] resulting in a slightly larger size in the DLS measurement. The reversible size change of PNIPAM-capped Au NPs upon repeated heating/cooling cycles was found, where their hydrodynamic diameters at 25°C and 50°C remained nearly unchanged. We note that as ATRP is a living polymerization technique and the dimension of the Au NP and PNIPAM ligand are governed by the MWs (i.e., length) of P*t*BA and PNIPAM, respectively, PNIPAM-capped Au NPs with varied size of Au NP and length of the PNIPAM ligand can be readily achieved using star-like PAA-*b*-PNIPAM with different MWs of P*t*BA and PNIPAM rendered by tuning the ATRP time of *t*BA and NIPAM monomers, respectively. For example, two new samples with the fixed diameter of Au NP of 14.6 nm ± 0.5 nm and the smaller thickness of PNIPAM ligands of 6.8 nm ± 0.3 nm and the smaller diameter of Au NP of 8.1 nm ± 0.4 nm and the further reduced thickness of PNIPAM ligands of 2.6 nm ± 0.1 nm have also been crafted.

Thermoresponsive optical property of PNIPAM-capped Au NPs in water was studied by UV-vis spectroscopy. Clearly, the PNIPAM-capped Au NP aqueous solution exhibited a characteristic surface plasmon resonance (SPR) peak of Au NP at 522 nm at 20°C. When the solution was heated, the SPR peak position gradually red-shifted from 522 nm to 532 nm accompanied by an increase in intensity (**Figure 1e**). As demonstrated in the TEM (**Figure 1b-d**) and DLS measurements as well as the literature on bulk PNIPAM,[3] the PNIPAM ligands underwent a volume transition during heating (**Figure 2a**). Accordingly, this resulted in an increase of the local refractive index of Au NPs and in turn the red-shift (as large as 10 nm) and the rising of the SPR peak, which can be predicted by Mie theory.[18,27] The inset in **Figure 1e** depicts the thermoresponsive optical properties of PNIPAM-capped Au NPs, where the variations of both the *absorbance@400 nm* and the SPR peak position λ_{max} are plotted against temperature. The absorbance at 400 nm is chosen to reflect the thermoresponsive optical property of PNIPAM-capped Au NPs because this wavelength corresponds primarily to the absorbance of Au atoms due to the interband transitions, and the absorbance will not red-shift even if Au NPs aggregate.[5,30] Intriguingly, the transition temperature (~32°C; LCST) in both *absorbance@400 nm* and λ_{max} plots (inset in **Figure 1e**) agreed qualitatively with that in the size evolution of PNIPAM-capped Au NPs measured by DLS. The SPR peak positions of PNIPAM-capped Au NPs can be readily switched between 522 nm and 532 nm by heating and cooling process, respectively, indicating a reversible thermoresponsive optical property due to the repeated collapse and stretching of intimately and permanently ligated PNIPAM chains on the Au NP surface. This contrasts sharply to poly(ethylene oxide) (PEO)-capped Au NPs where no obvious spectral change was observed, further substantiating that the thermally responsive optical property was originated from the ligated PNIPAM shell as PEO is a non-thermoresponsive polymer.

As discussed above, the PNIPAM-capped Au NP system is free of any possible linear PNIPAM chains detached from the NP surface. On the basis of the results described above (i.e., reduced thickness of the PNIPAM ligands from 10.6 nm at 25°C to 5.8 nm at 50°C as evidenced by TEM (**Figure 1b-d**), reduced diameter of PNIPAM-capped Au NPs in water as temperature continuously increased from 10 °C to 50 °C as assessed by DLS, together with the red-shift and enhancement of the SPR peak as measured by UV-vis spectroscopy (**Figure 1e**)), it is clear that upon heating the PNIPAM ligands are collapsed on the Au NP surface without the aggregation of neighboring Au NPs.

We now turn our attention to the situation where free linear PNIPAM chains were deliberately added to the PNIPAM-capped Au NP aqueous solution. Linear PNIPAM (M_n = 24,700) was prepared by a similar ATRP procedure using EBIB as the initiator. As our nanoreactor strategy ensures no detachment of PNIPAM ligands from the Au NP surface, the amount of free PNIPAM chains intentionally added to the system can be accurately controlled and quantified to trigger the aggregation of PNIPAM-capped Au NPs upon heating. Briefly, a small amount of free linear PNIPAM was added to the PNIPAM-capped Au NPs solution at 25°C. After complete dissolution, the system was heated above LCST and centrifuged at 4000 × g for 1 min to remove the aggregated PNIPAM-capped Au NPs. The supernatant (i.e., dispersed Au NPs) was then collected and cooled to 25°C, and measured by UV-vis spectroscopy. As the concentration of the Au NPs dispersed in supernatant is proportional to their absorption, the magnitude of precipitation can be readily tracked by monitoring the absorbance of supernatants at 400 nm. An obvious decrease in absorbance occurred when the amount of added free linear PNIPAM increased, revealing that the PNIPAM-capped Au NPs partially precipitated and thus the Au NP concentration in the supernatant was reduced. To this end, 0.081 mM (i.e., 2 mg mL^{-1}) and 0.182 mM (i.e., 4.5 mg mL^{-1}) of free linear PNIPAM were selected as two representative cases to insufficiently and adequately, respectively, cause PNIPAM-capped Au NPs to aggregate and precipitate.

Figure 3a-c shows the thermoresponse of PNIPAM-capped Au NPs in the presence of a small amount of added linear PNIPAM chains (i.e., 0.081 mM) to trigger insufficient aggregation of NPs. The PNIPAM-capped Au NPs are monodisperse and isolated at 25°C even with the free linear PNIPAM present (**Figure 3a**). When heated to 50°C, the Au NPs clearly aggregated (**Figure 3b**), which can be reversed upon cooling (**Figure 3c**). The hydrodynamic diameter of PNIPAM-capped Au NPs measured by DLS displayed a size increase from 79 nm to around 200 nm as a function of temperature from 20°C to 50°C, suggesting that the free linear PNIPAM chains added may perform as a physical crosslinker between adjacent PNIPAM-capped Au NPs due to the favorable enthalpic interaction of PNIPAM ligands with free linear PNIPAM chains,[31,32] leading to the aggregation of PNIPAM-capped Au NPs above LCST, as schematically illustrated in **Figure 2b**. Nonetheless, the size of PNIPAM-capped Au NPs exhibited a high reversibility upon the heating/cooling cycle.

Figure 3d presents the thermoresponsive optical properties of the PNIPAM-capped Au NP aqueous solution with a small amount of free linear PNIPAM chains added (i.e., 0.081

mM). The SPR peak position red-shifted by 15 nm from 522 nm to 537 nm accompanied by a decrease in peak intensity and a broadening in full-width-at-half-maximum (FWHM) upon heating yet reversible upon cooling. The red-shift and the peak broadening with temperature are due to the collective electromagnetic response of aggregated Au NPs to the incident light.[7,33-35] Moreover, owing to the screening of Au NPs embedded within the aggregate, their full illumination is restricted, resulting in a reduced SPR peak intensity.[7,33-35] It is interesting to note that in the absence of free PNIPAM chains in the solution, no obvious change was observed by naked eyes during heating, which is consistent with the results (**Figures 1b-e**) of no aggregation occurring. With the addition of a small amount of free linear PNIPAM (i.e., 0.081 mM), a slight change in solution color and turbidity was seen at 50°C. Nevertheless, in both cases no precipitation was observed on the bottom of the solution. Notably, the deliberately introduced free linear PNIPAM chains can be readily removed completely by ultracentrifugation due to its much lower density than PNIPAM-capped Au NPs, and the precipitated PNIPAM-capped Au NPs can be re-dissolved in water with no visible change in the solution color and transparency comparable to the original linear PNIPAM-free solution. Clearly, two different thermoresponsive optical properties can be achieved and switched by simply controlling the presence of free linear PNIPAM in the system.

Intrigued by the results on the PNIPAM-capped Au NP aqueous solution added with a small amount of free linear PNIPAM, we set out to investigate the situation where a large amount of free linear PNIPAM introduced (i.e., 0.182 mM). **Figure 3e** shows a representative TEM image of the sample at 25 °C. Although the Au NPs were embedded within the matrix of free PNIPAM chains, they remained monodisperse without aggregation. At the temperature below the LCST, the solution appeared similarly to the previous two cases. When the temperature was above the LCST, instead of a homogeneous film, a dense PNIPAM matrix with an irregular shape was seen (**Figure 3f**), where the Au NPs were trapped within the PNIPAM matrix and appeared darker in close-up TEM (inset). Thus, the system was no longer soluble and precipitated on the bottom. Notably, this process was reversible upon cooling (**Figure 3g**). The temperature dependence of the system was further studied by DLS. Despite that PNIPAM-capped Au NPs can still dissolve individually at 20°C, their size dramatically increased to 1220 nm around the LCST, implying that PNIPAM-capped Au NPs in the presence of 0.182 mM (i.e., 4.5 mg mL^{-1}) of free PNIPAM added can easily aggregate to form a large size above the LCST and precipitate. The corresponding thermally responsive optical properties were then scrutinized by UV-vis spectroscopy (**Figure 3h**). As the temperature increased from 20°C to 50°C, the intensity of the SPR peak originally located at 522 nm at 20°C gradually decreased, followed by slight red-shift and peak broadening, and a broad second peak at the longer wavelength gradually developed. This new peak can be attributed to the heavily aggregated Au NPs in the added linear PNIPAM homopolymer matrix,[36] as illustrated in **Figure 2c**. The free linear PNIPAM and PNIPAM-capped Au NPs can be readily separated by ultracentrifugation on the basis of their large density difference. Instead of an isolated-to-aggregated transition, after removing the excess free linear PNIPAM by centrifugation, the PNIPAM-capped Au NPs redispersed in water were found to exhibit a swollen-to-collapsed shell transition.

The significance of the added linear PNIPAM in producing the aggregated PNIPAM-capped Au NPs discussed above can be further substantiated by performing a control experiment where free linear PNIPAM chains was replaced with free linear PEO chains of similar molecular weight. Unlike linear PNIPAM, no obvious change in the solution color and transparency was observed in the case of adding linear PEO due to the lack of thermoresponsiveness of PEO at temperature either above or below the LCST of PNIPAM. This observation corroborated that the importance of free linear PNIPAM in triggering the aggregation of PNIPAM-capped Au NPs (**Figures 3e-h**).

In addition to thermoresponsive optical properties, the temperature-dependent catalytic activity of PNIPAM-capped Au NPs was also evaluated using the reduction of 4-nitrophenol (4-NP) to 4-aminophenol (4-AP) by $NaBH_4$ as a model reaction. The pollutant nature of nitrophenol and its derivatives (e.g., 4-NP) has been a big public concern.[37] On the other hand, there is a great demand for the reduction product 4-AP for use as corrosion inhibitor and in pharmaceutical industry.[37] Clearly, this reduction reaction is of importance for fundamental study and technological applications. The 4-NP aqueous solution under neutral or acidic condition had a characteristic absorption peak at 317 nm. The use of $NaBH_4$ led to the formation of 4-nitrophenolate ions under the alkaline condition, accompanied with a red-shift from 317 nm to 400 nm.[37,38] No obvious change in the absorbance at 400 nm over 24 hrs was seen, indicating that no reaction occurred in the absence of a catalyst. In contrast, in the absence of free linear PNIPAM, the addition of PNIPAM-capped Au NPs resulted in a rapid decrease in the peak intensity at 400 nm with the emergence of a new peak at 295 nm assigned to 4-AP. As the peak intensity at 400 nm was much stronger than that of 295 nm, the proceeding of the reaction was monitored by measuring the absorbance at 400 nm over time, reflecting the change in the concentration C of 4-NP. As only a small amount of PNIPAM-capped Au NPs (~ 9.62×10^{-4} g·L^{-1} for Au) was employed to catalyze the reduction of 4-NP, the influence of Au NPs on the absorbance and scattering was neglected.[39] Due to the excess of $NaBH_4$ over 4-NP in the reaction system, the concentration of $NaBH_4$ was nearly unchanged. Thus, the reaction was pseudo-first-order with respect to the concentration of 4-NP (in the 4-nitrophenolate ion form),[37-40] as shown in equation (1).

$$-\frac{dC_t}{dt} = k_{app}C_t = k_1 S C_t \quad (1)$$

where C_t is the concentration of 4-NP at time t, the apparent kinetic rate constant k_{app} is strictly proportional to the surface area of the metal NPs in the system,[37] k_1 is the rate constant normalized to S, and S is the surface area of the metal NPs normalized to the unit volume of the system.

Figure 4a shows the ln (C_t/C_0) plotted as a function of time at different temperatures from 10°C to 50°C. Notably, an induction period t_0 can be obtained via extrapolation to zero conversion at all temperatures, which may be likely due to the reduction of oxygen in the system.[37,41] As $NaBH_4$ was in a large excess, its consumption by oxygen can be neglected. The dependence of $1/t_0$ on temperature approximately followed the Arrhenius law.[41] The k_{app} at 25°C was found to be 4.30×10^{-3} s^{-1}, consistent with the reported values in the literature. The calculated k_1 of 2.1×10^{-1} s^{-1}·m^{-2}·L was either comparable or higher than the other

reported Au NP systems. The improved catalytic performance can be attributed to the large accessibility of the NP surface imposed by the expanded yet ligated PNIPAM chains. It is interesting to note that similar catalytic activities were seen in other metal NPs (e.g., Pd, Pt, Ag) templated by dendrimers[42,43] and brushes.[2,41]

Quite intriguingly, the apparent kinetic rate constants k_{app} do not present a conventional Arrhenius-type dependence on temperature. Rather than a familiar linear relationship in the ln $k_{app} \sim 1/T$ plot, three regions were observed as shown in **Figure 4b**, displaying a non-monotonic behavior. Such catalytic activity represents a delicate balance between the diffusion rate of the reactant which relies on the temperature-dependent transition of PNIPAM shell and the thermoactivity of the catalytic reduction which increases with temperature.[37,41,44] The corresponding volume ($\sim R_h^3$) change of the PNIPAM shell is also shown in **Figure 4b**, where R_h is the hydrodynamic radius of PNIPAM-capped Au NPs (R_h = ½ D_h). When the temperature was low, the reactants (i.e., 4-NP) for the catalytic reduction can diffuse freely through the expanded PNIPAM shell and reach the Au NP surface.[44] Thus, the k_{app} followed a typical Arrhenius-type behavior over temperature. As the temperature increased from 25°C to 37.5°C, the PNIPAM ligands contracted significantly as reflected in a large decrease in volume of PNIPAM-capped Au NPs (blue squares in **Figure 4b**). Such temperature-triggered shrinkage of the PNIPAM shell impeded the diffusion of the reactants to the Au NP surface (i.e., reduced accessibility).[44] This effect dominates over the thermoactivity of the catalytic reduction, thereby resulting in an overall decreased k_{app}. Further increasing the temperature from 37.5°C to 50°C, the PNIPAM shell only slightly shrunk and eventually remained unchanged, during which the diffusional barrier imposed by collapsed PNIPAM chains is overcome by the elevated temperature. As a result, the thermal activity of the catalytic reduction increased, leading to the rising of k_{app} again. The colloidal stability of PNIPAM-capped Au NPs after catalytic reduction was confirmed by TEM, where NPs remained well-dispersed with retained size and shape, instead of increased size after catalytic reduction by $NaBH_4$ as seen in thiol-capped Au NPs.[45] Clearly, the PNIPAM ligands improved the Au NP stability.

On the other hand, when a large amount of free linear PNIPAM was added into the PNIPAM-capped Au NP water solution, the PNIPAM-capped Au NPs possessed an isolated-to-aggregated transition as discussed above. In this case, when the catalytic reduction was performed below the LCST (i.e., at T = 10 °C, 15 °C, 20 °C and 25 °C), the obtained k_{app} (**Figure 4c**) is similar to those of the system in the absence of free linear PNIPAM chains (**Figure 4a**), suggesting the catalytic activity of PNIPAM-capped Au NPs was not greatly affected by free linear PNIPAM chains below the LCST. However, as the temperature was heated above the LSCT, for instance, 50 °C, the k_{app} decreased from 4.34×10^{-3} s^{-1} to 3.28×10^{-5} s^{-1} calculated from **Figure 4c**. The high k_{app} was resumed once the temperature returned below the LCST. On the basis of these observations, an "on/off" catalytic behavior readily regulated by temperature can thus be achieved (**Figure 4d**). The on-to-off ratio, $k_{app,on}/k_{app,off}$, was found to be ~132, one order of magnitude higher than those reported thermo-[21,46] and photo-responsive[47,48] systems.

It is well-known that the catalytic reduction occurs on the NP surface and the catalytic activity under certain temperature relies on the total accessible surface area S_{tol}. In the presence of a large amount of free linear PNIPAM, when the temperature was above the LCST, the PNIPAM-capped Au NPs eventually aggregated and precipitated. This led to a dramatic decrease of S_{tol}, and accordingly the arrest of the 4-NP reduction. Thus, the catalytic reduction can be easily modulated "on" and "off" across the LCST. We note that the free linear PNIPAM chains added can be readily removed by centrifugation due to the significant density difference between PNIPAM and PNIPAM-capped Au NPs. Therefore, the switching between "on/off" and non-monotonic catalytic modes can be conveniently achieved by controlling the presence of free linear PNIPAM in the system.

Conceptually, as proper precursors amenable to the star-like block copolymer nanoreactor strategy are unlimited, in addition to Au NPs, a rich variety of monodisperse PNIPAM-capped NPs can be conveniently crafted, including, plasmonic Ag, semiconducting TiO_2, insulating SiO_2, magnetic Fe_3O_4, and ferroelectric $BaTiO_3$ NPs (TEM images in **Figure 5**). Such hybrid materials may render the scrutiny of the synergistic coupling between inorganic NPs and organic polymer ligands without the concern for ligand dissociation.

Conclusion

In summary, two widely recognized contradictory observations in the literature on temperature-dependent optical (i.e., *small* vs. *large* red-shift of the SPR peak) and catalytic (*non-monotonic* vs. "*on/off*") properties of thermoresponsive Au NPs as temperature rises over the LCST are reconciled by capitalizing on judiciously crafted PNIPAM-capped Au NPs. We note that the dynamic dissociation of PNIPAM ligands of the Au NP surface may account for such controversial reports in the past work. In stark contrast, PNIPAM-capped Au NPs templated by exploiting rationally designed star-like diblock copolymers as nanoreactors render the intimate and permanent tethering of thermoresponsive PNIPAM chains, thereby eliminating the possible detachment of PNIPAM during purification, storage and heating/cooling cycles of NPs, and thus ensuring good control over the thermoresponsive optical and catalytic properties of PNIPAM-capped Au NPs with high reversibility. As-prepared PNIPAM-capped Au NPs exhibit small red-shift of the SPR peak and non-monotonic (i.e., non-Arrhenius) catalytic activity. Intriguingly, the addition of a large amount of free linear PNIPAM into the PNIPAM-capped Au NPs results in a large red-shift of the SPR peak and an "on/off" catalytic property.

The star-like block copolymer nanoreactor strategy we developed is general and robust. As demonstrated, it renders the crafting of a myriad of thermoresponsive polymer-capped functional NPs, such as Ag, TiO_2, Fe_3O_4, and $BaTiO_3$, to explore their intriguing coupling properties (i.e., thermoresponsive/plasmonic, thermoresponsive/catalytic, thermoresponsive/magnetic, and thermoresponsive/ferroelectric, respectively). Moreover, stimuli-responsive but thermoresponsive polymers can also be conveniently introduced during the synthesis of star-like block copolymer nanoreactors to create light- and pH-responsive functional NPs for a wide range of applications in smart materials and devices.

References

1. Liu, T.-Y.; Hu, S.-H.; Liu, D.-M.; Chen, S.-Y.; Chen, I.-W., *Nano Today* **2009,** *4* (1), 52-65.
2. Lu, Y.; Ballauff, M., *Prog. Polym. Sci.* **2011,** *36* (6), 767-792.
3. Pelton, R., *Adv. Colloid Interface Sci.* **2000,** *85* (1), 1-33.
4. Kim, D. J.; Kang, S. M.; Kong, B.; Kim, W. J.; Paik, H. J.; Choi, H.; Choi, I. S., *Macromol. Chem. Phys.* **2005,** *206* (19), 1941-1946.
5. Jones, S. T.; Walsh-Korb, Z.; Barrow, S. J.; Henderson, S. L.; del Barrio, J. s.; Scherman, O. A., *ACS Nano* **2016,** *10* (3), 3158-3165.
6. Zhu, M.-Q.; Wang, L.-Q.; Exarhos, G. J.; Li, A. D., *J. Am. Chem. Soc.* **2004,** *126* (9), 2656-2657.
7. Chen, Y.; Wang, Z.; He, Y.; Yoon, Y. J.; Jung, J.; Zhang, G.; Lin, Z., *Proc. Natl. Acad. Sci. U. S. A.* **2018,** *115*, E1391-E1400.
8. Love, J. C.; Estroff, L. A.; Kriebel, J. K.; Nuzzo, R. G.; Whitesides, G. M., *Chem. Rev.* **2005,** *105* (4), 1103-1170.
9. Ling, D.; Hackett, M. J.; Hyeon, T., *Nano Today* **2014,** *9* (4), 457-477.
10. Niu, Z.; Li, Y., *Chem. Mater.* **2013,** *26* (1), 72-83.
11. Dong, H.; Zhu, M.; Yoon, J. A.; Gao, H.; Jin, R.; Matyjaszewski, K., *J. Am. Chem. Soc.* **2008,** *130* (39), 12852-12853.
12. Kim, J.-B.; Bruening, M. L.; Baker, G. L., *J. Am. Chem. Soc.* **2000,** *122* (31), 7616-7617.
13. Zheng, P.; Jiang, X.; Zhang, X.; Zhang, W.; Shi, L., *Langmuir* **2006,** *22* (22), 9393-9396.
14. Pang, X.; Zhao, L.; Akinc, M.; Kim, J. K.; Lin, Z., *Macromolecules* **2011,** *44* (10), 3746-3752.
15. Vriezema, D. M.; Comellas Aragonès, M.; Elemans, J. A.; Cornelissen, J. J.; Rowan, A. E.; Nolte, R. J., *Chem. Rev.* **2005,** *105* (4), 1445-1490.
16. Leong, W. L.; Lee, P. S.; Lohani, A.; Lam, Y. M.; Chen, T.; Zhang, S.; Dodabalapur, A.; G Mhaisalkar, S., *Adv. Mater.* **2008,** *20* (12), 2325-2331.
17. Gibson, M. I.; O'Reilly, R. K., *Chem. Soc. Rev.* **2013,** *42* (17), 7204-7213.
18. Contreras Cáceres, R.; Sánchez Iglesias, A.; Karg, M.; Pastoriza Santos, I.; Pérez Juste, J.; Pacifico, J.; Hellweg, T.; Fernández Barbero, A.; Liz Marzán, L. M., *Adv. Mater.* **2008,** *20* (9), 1666-1670.
19. Carregal-Romero, S.; Buurma, N. J.; Pérez-Juste, J.; Liz-Marzán, L. M.; Hervés, P., *Chem. Mater.* **2010,** *22* (10), 3051-3059.
20. Ding, T.; Valev, V. K.; Salmon, A. R.; Forman, C. J.; Smoukov, S. K.; Scherman, O. A.; Frenkel, D.; Baumberg, J. J., *Proc. Natl. Acad. Sci. U. S. A.* **2016,** *113* (20), 5503-5507.
21. Jiang, X.; Xiong, D. A.; An, Y.; Zheng, P.; Zhang, W.; Shi, L., *J. Polym. Sci., Part A: Polym. Chem.* **2007,** *45* (13), 2812-2819.
22. Pang, X.; Zhao, L.; Feng, C.; Lin, Z., *Macromolecules* **2011**, *44* (18), 7176-7183.
23. Xu, H.; Xu, Y.; Pang, X.; He, Y.; Jung, J.; Xia, H.; Lin, Z., *Sci. Adv.* **2015,** *1* (2), e1500025.
24. Pang, X.; He, Y.; Jung, J.; Lin, Z., *Science* **2016,** *353* (6305), 1268-1272.
25. Matyjaszewski, K.; Tsarevsky, N. V., *Nat. Chem.* **2009,** *1* (4), 276-288.
26. Chen, Y.; Yang, D.; Yoon, Y. J.; Pang, X.; Wang, Z.; Jung, J.; He, Y.; Harn, Y. W.; He, M.;

Zhang, S., *J. Am. Chem. Soc.* **2017,** *139* (37), 12956-12967.
27. Chen, Y.; Yoon, Y. J.; Pang, X.; He, Y.; Jung, J.; Feng, C.; Zhang, G.; Lin, Z., *Small* **2016,** *12* (48), 6714-6723.
28. Tang, F.; Ma, N.; Wang, X.; He, F.; Li, L., *J. Mater. Chem.* **2011,** *21* (42), 16943-16948.
29. Cho, E. C.; Lee, J.; Cho, K., *Macromolecules* **2003,** *36* (26), 9929-9934.
30. Kimling, J.; Maier, M.; Okenve, B.; Kotaidis, V.; Ballot, H.; Plech, A., *J.Phys. Chem. B* **2006,** *110* (32), 15700-15707.
31. Schild, H. G., *Prog. Polym. Sci.* **1992,** *17* (2), 163-249.
32. Yan, J.; Kristufek, T.; Schmitt, M.; Wang, Z.; Xie, G.; Dang, A.; Hui, C. M.; Pietrasik, J.; Bockstaller, M. R.; Matyjaszewski, K., *Macromolecules* **2015,** *48* (22), 8208-8218.
33. Storhoff, J. J.; Lazarides, A. A.; Mucic, R. C.; Mirkin, C. A.; Letsinger, R. L.; Schatz, G. C., *J. Am. Chem. Soc.* **2000,** *122* (19), 4640-4650.
34. Lazarides, A. A.; Schatz, G. C., *J.Phys. Chem. B* **2000,** *104* (3), 460-467.
35. Jin, R.; Wu, G.; Li, Z.; Mirkin, C. A.; Schatz, G. C., *J. Am. Chem. Soc.* **2003,** *125* (6), 1643-1654.
36. Jiang, Y.; Zhao, H.; Zhu, N.; Lin, Y.; Yu, P.; Mao, L., *Angew. Chem. Int. Ed.* **2008,** *47* (45), 8601-8604.
37. Panigrahi, S.; Basu, S.; Praharaj, S.; Pande, S.; Jana, S.; Pal, A.; Ghosh, S. K.; Pal, T., *J.Phys. Chem. C* **2007,** *111* (12), 4596-4605.
38. Seo, E.; Kim, J.; Hong, Y.; Kim, Y. S.; Lee, D.; Kim, B.-S., *J.Phys. Chem. C* **2013,** *117* (22), 11686-11693.
39. Lu, Y.; Mei, Y.. *Angew. Chem. Int. Ed.* **2006,** *45* (5), 813-816.
40. Pradhan, N.; Pal, A.; Pal, T., *Colloids Surf. A Physicochem. Eng. Asp.* **2002,** *196* (2-3), 247-257.
41. Lu, Y.; Mei, Y.; Walker, R.; Ballauff, M.; Drechsler, M., *Polymer* **2006,** *47* (14), 4985-4995.
42. Zhao, M.; Crooks, R. M., *Angew. Chem. Int. Ed.* **1999,** *38* (3), 364-365.
43. Crooks, R. M.; Zhao, M.; Sun, L.; Chechik, V.; Yeung, L. K., *Acc. Chem. Res.* **2001,** *34* (3), 181-190.
44. Álvarez Puebla, R. A.; Contreras Cáceres, R.; Pastoriza Santos, I.; Pérez Juste, J.; Liz Marzán, L. M., *Angew. Chem. Int. Ed.* **2009,** *48* (1), 138-143.
45. Dasog, M.; Hou, W.; Scott, R. W., *Chem. Commun.* **2011,** *47* (30), 8569-8571.
46. Wang, Q.; Wang, J.; Wang, D.; Turhong, M.; Zhang, M., *Chem. Eng. J.* **2015,** *280*, 158-164.
47. Keiper, S.; Vyle, J. S., *Angew. Chem. Int. Ed.* **2006,** *45* (20), 3306-3309.
48. Fruk, L.; Rajendran, V.; Spengler, M.; Niemeyer, C. M., *ChemBioChem* **2007,** *8* (18), 2195-2198.

Figures and Figure Captions

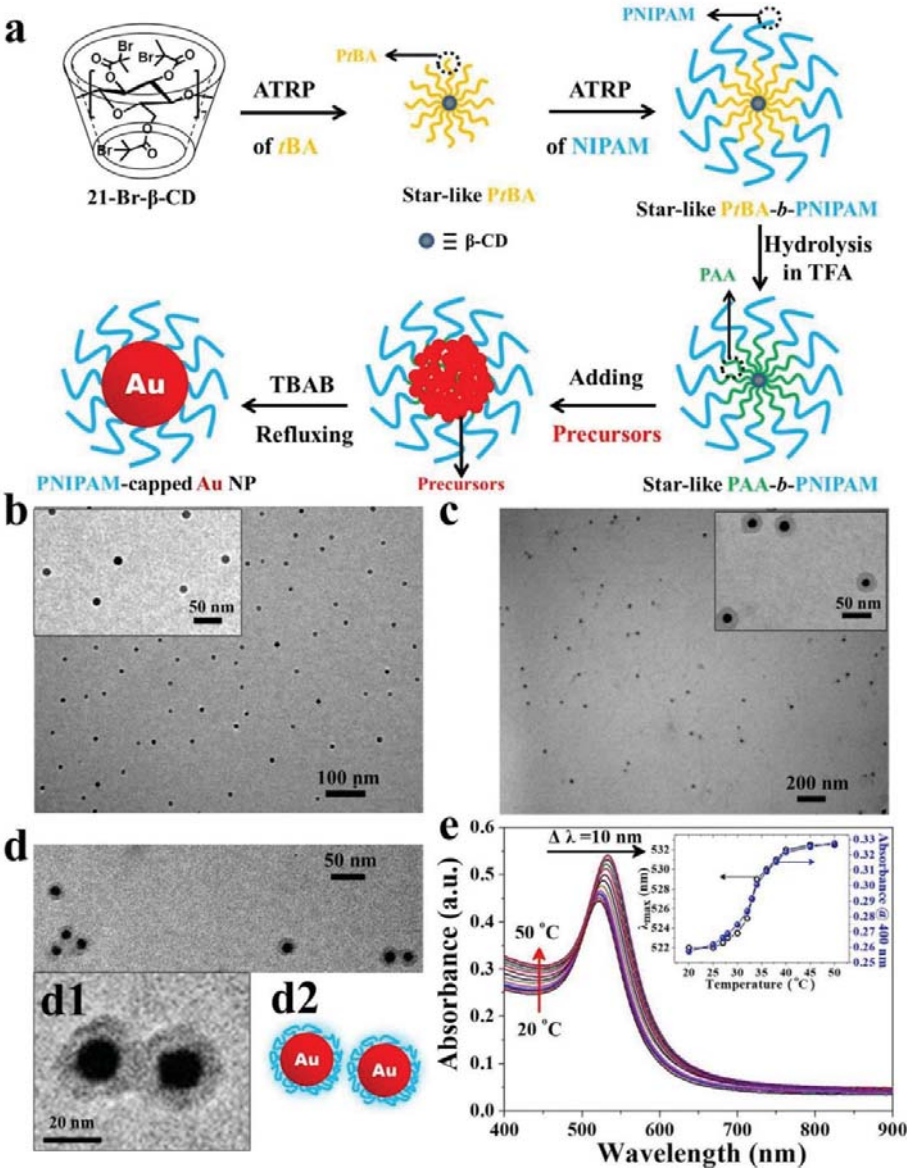

Figure 1. (a) Synthetic route to Au NP *intimately* and *permanently* ligated by thermoresponsive PNIPAM via capitalizing on star-like PAA-*b*-PNIPAM diblock copolymer as nanoreactor (i.e., yielding PNIPAM-capped Au NP). (b-d) TEM images of PNIPAM-capped Au NPs (c = 1 mg mL^{-1}): (b) without staining at 25 °C, (c) after staining at 25 °C, and (d) after staining at 50 °C. Prior to staining, no PNIPAM ligands can be seen as shown in inset in (b). After staining, PNIPAM ligands form a relatively light shell on the surface of Au NP, which can be visualized as shown in inset in (c) and (d1). A schematic of two Au NPs in close proximity, corresponding to (d1), is shown in (d2). (e) UV-vis spectra of the PNIPAM-capped Au NPs aqueous solution (c =1 mg mL^{-1}) as temperature increases from 20°C to 50°C. The inset shows the evolutions of both the SPR peak position (λ_{max}) and the absorbance at 400 nm (*Absorbance@400 nm*) as a function of temperature.

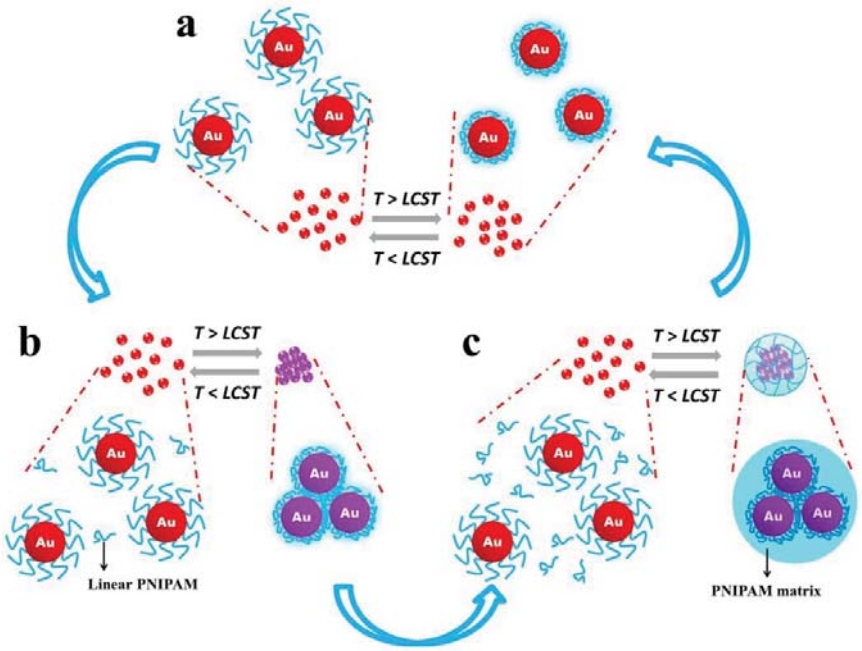

Figure 2. Schematic illustration of the PNIPAM-capped Au NP aqueous solution experiencing reversible thermal transition across LCST. (a) Extension-to-shrinkage transition of PNIPAM shell in the absence of free linear PNIPAM chains. (b) Dispersion-to-aggregation transition of NPs in the presence of a small amount of deliberately added linear PNIPAM chains. (c) Dispersion-to-precipitation transition of NPs in the presence of an excess amount of deliberately added linear PNIPAM chains.

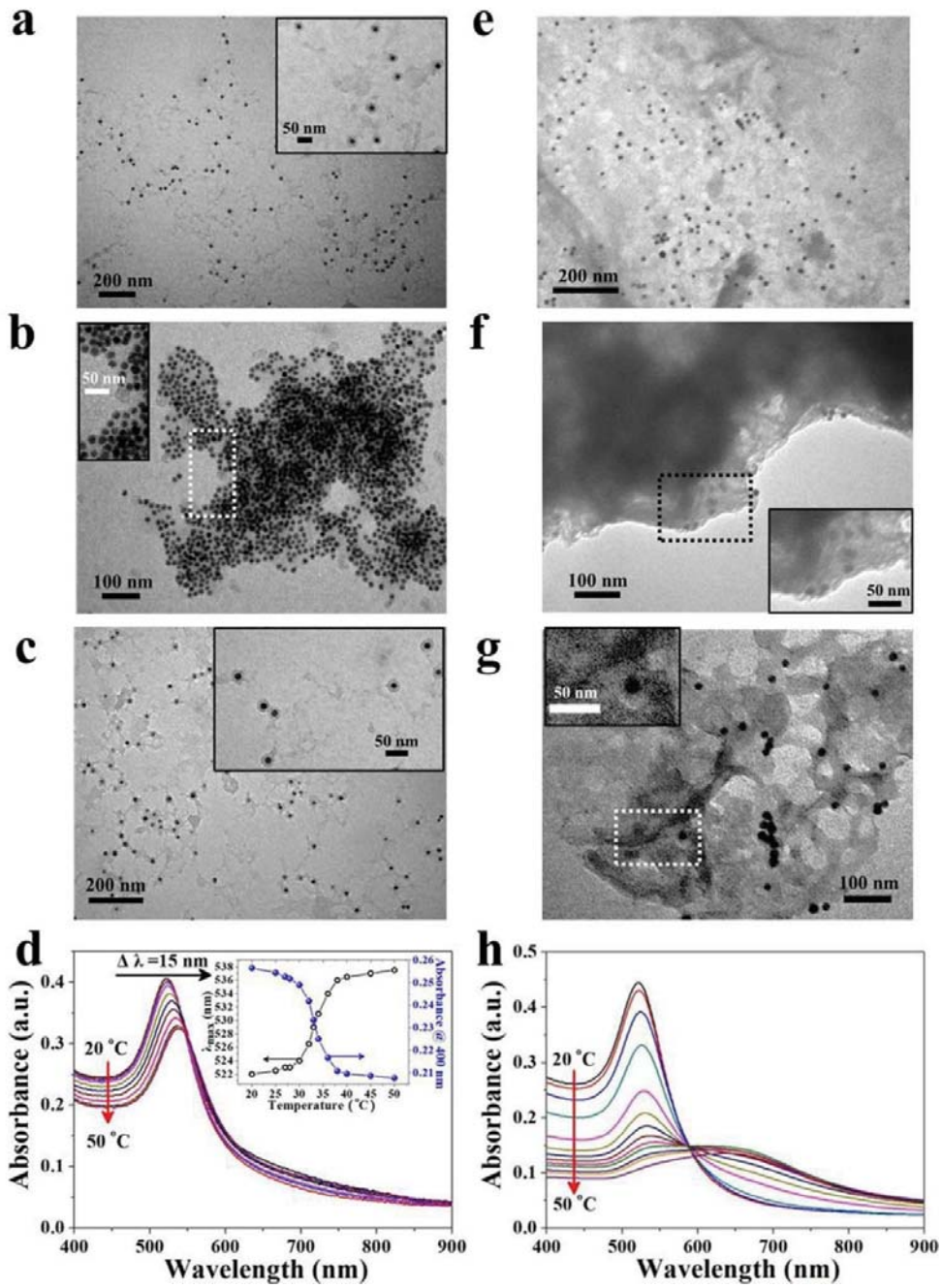

Figure 3. (a-c) TEM images and (d) UV-vis spectra from 20°C to 50°C of PNIPAM-capped Au NPs (c =1 mg mL^{-1}) with the presence of 0.081 mM (i.e., 2 mg mL^{-1}; a small amount) of free linear PNIPAM. (a) At 25°C, (b) heating to 50 °C, and (c) cooling back to 25°C. The inset in (d) shows the evolutions of both the SPR peak position (λ_{max}) and the absorbance at 400 nm (*Absorbance@400 nm*) as a function of temperature. (e-g) TEM images and (h) UV-vis spectra from 20°C to 50°C of PNIPAM-capped Au NPs (c = 1 mg mL^{-1}) with the presence of 0.182 mM (i.e., 4.5 mg mL^{-1}; a large amount) of free linear PNIPAM. (e) At 25°C, (f) heating to 50°C, and (g) cooling back to 25°C. All TEM samples are stained prior to imaging.

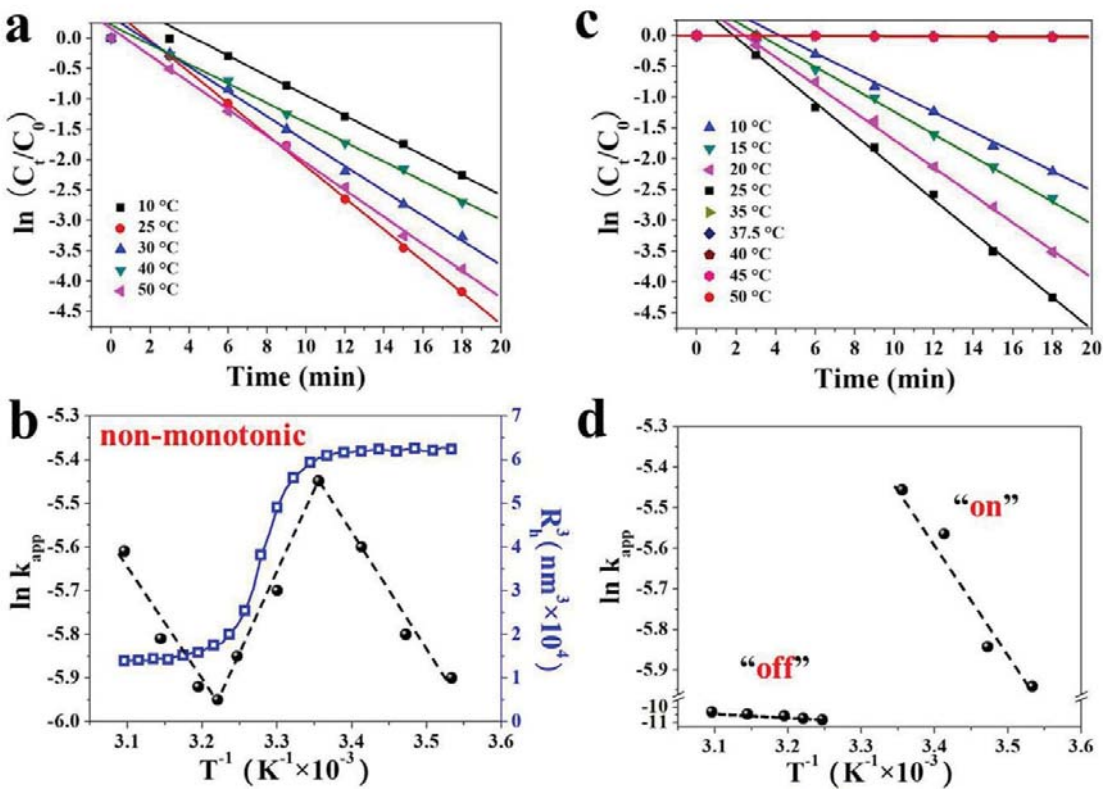

Figure 4. Control between non-monotonic and "on/off" catalytic activities enabled by switchable thermoresponsive behaviors of PNIPAM-capped Au NPs. (a) Non-monotonic catalytic activity and (b) corresponding Arrhenius plot of the apparent kinetic rate constant k_{app} of PNIPAM-capped Au NPs in reducing 4-NP into 4-AP in the absence of free linear PNIPAM. The corresponding volume change of PNIPAM shell represented by R_h^3 (blue squares). (c) "On/off" catalytic activity and (d) corresponding Arrhenius plot of k_{app} of PNIPAM-capped Au NPs in the presence of a large amount of linear PNIPAM (0.182 mM) at temperatures below and above the LCST, respectively. The initial concentrations are: [4-NP] = 10^{-4} M, [$NaBH_4$] = 6.67×10^{-3} M, and [Au] = 9.62×10^{-4} g·L^{-1}.

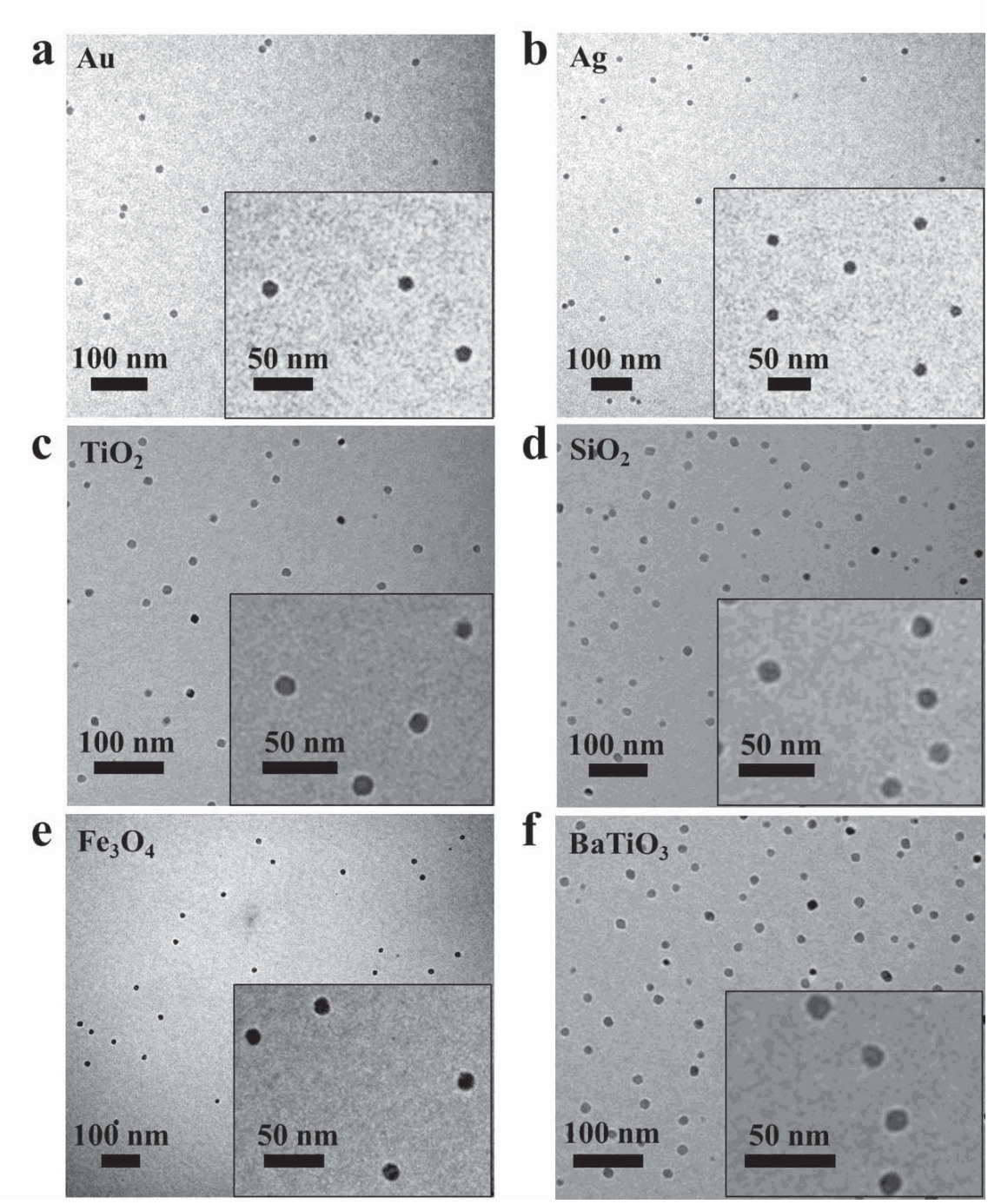

Figure 5. Representative TEM images of a set of PNIPAM-capped NPs in-situ crafted using star-like PAA-*b*-PNIPAM as nanoreactors. (a) Plasmonic Au, (b) plasmonic Ag, (c) semiconducting TiO_2, (d) insulating SiO_2, (e) magnetic Fe_3O_4, and (f) ferroelectric $BaTiO_3$ NPs.

Part B: Enabling Tailorable Optical Properties and Markedly Enhanced Stability of Perovskite Quantum Dots by Permanently Ligating with Polymer Hairs

Advanced Materials (revised manuscript submitted)

Perovskites represent an emerging class of materials by a generic chemical formula ABX_3 with A^+ = methylammonium ($CH_3NH_3^+$), formamidinium ($HC(NH_2)_2^+$), Cs, or their combination; $B^{2+} = Pb^{2+}$ and/or Sn^{2+}; $X^- = Cl^-$, Br^- and/or I^-. Recently, perovskite quantum dots (QDs) has garnered tremendous attention owing to their broad visible-to-near infrared wavelength tunability (400-800 nm) and narrow band emission[1-4] for use in lasers,[5] electroluminescence devices,[2, 6] sensors,[7] and solar cells.[3] Among perovskite QDs, all-inorganic $CsPbX_3$ QDs possess narrow FWHM of emission (as small as 12 nm) and excellent quantum yield (QY; 50%~90%).[1, 8] They have a Bohr diameter up to 12 nm,[1] exhibiting a size-tunable bandgap in the visible region. It is also notable that the exchange of halide ions (Cl^-, Br^- and I^-) in as-synthesized perovskite QDs is highly effective, rendering easy and rapid access to a wide range of perovskite QDs with tunable absorption and photoluminescence (PL) spectra.[1]

In spite of significant advances in perovskite research noted above, a key to the success of perovskite-based materials and devices is the stability of perovskites as they are susceptible to decomposition due to their ionic crystal nature.[7, 9] Recently, several methods including coating with alumina by atomic layer deposition,[10] partial coating with SiO_2 via sol-gel process,[11] physical mixing with hydrophobic polymers,[12] and encapsulation within mesoporous silica[7] or polymer beads[13] have proven to be effective in improving stability in polar and ambient environments. However, nearly all approaches described above for stability enhancement result in nanocomposites with multiple perovskite QDs encapsulated in microscopic protective matrices. These microscale nanocomposites may be disadvantageous for biomedical applications where cellular uptake is more feasible for smaller nanoscopic particles,[14] or LEDs where the processing of nanoscopic luminescent particles often leads to low scattering loss, higher loading and packing density and thus film uniformity.[11] Clearly, the ability to deliberately and reliably improve the stability of perovskite QDs (e.g., against humidity and polar solvents) while retaining their individual nanometer size represents a critical step that underpins future advances in optoelectronic and biological applications.

Herein, we report a general and robust strategy by capitalizing on judiciously designed amphiphilic star-like diblock copolymers with well-controlled molecular weight and low polydispersity of each block as molecularly engineered nanoreactors to craft uniform perovskite QDs. Remarkably, these QDs simultaneously possess precisely tunable dimensions and considerably enhanced colloidal and water stabilities via an extremely facile and rapid co-precipitation reaction. The amphiphilic star-like diblock copolymer nanoreactors exploited are poly(acrylic acid)-*block*-polystyrene (denoted PAA-*b*-PS) synthesized by atom transfer radical polymerization (ATRP), comprising hydrophilic inner PAA and hydrophobic outer PS block of different lengths. The selective partition of precursors within the compartment occupied by PAA blocks of star-like diblock copolymers due to strong coordination interaction between the carboxylic acid groups of PAA blocks in star-like PAA-*b*-PS nanoreactors and perovskite precursors yields *in-situ* hairy all-inorganic perovskite $CsPbX_3$ QDs perpetually ligated by hydrophobic PS blocks. It is noteworthy that the molecular weight of PAA and PS blocks can be readily tuned by varying their respective ATRP reaction times. This, in turn, presents twofold advantages, that is, simple yet reliable

control over the diameter of $CsPbX_3$ QDs governed by the length of the inner PAA blocks, thereby leading to precisely size-tunable optical properties, and concurrently outstanding water and colloidal stabilities of $CsPbX_3$ QDs dictated by the length of the outer PS blocks. It is important to note that the outer PS blocks are originally covalently connected to the inner PAA blocks, so the surface capping of $CsPbX_3$ QDs with PS blocks is intimate and permanent, ensuring excellent colloidal stability in nonpolar solvents and preventing QDs from aggregation. This contrasts sharply to conventional ligand-assisted methods, where ligands are non-covalently bonded to QDs, thus promoting agglomeration of QDs due to the dynamic association-dissociation of surface ligands over time. Moreover, the permanently attached outer PS block forms a protective hydrophobic shell around perovskite QD where the thickness of shell depends on the length of PS blocks, thereby assuring greatly enhanced stability against polar solvents (e.g., water).

Results and Discussion

Figure 1 depicts the synthetic route to hairy all-inorganic perovskite QDs intimately and permanently ligated by PS chains via capitalizing on amphiphilic unimolecular star-like PAA-*b*-PS diblock copolymers as nanoreactors, where the formation of $CsPbBr_3$ QD is taken as an example. First, a series of star-like poly(*tert*-butyl acrylate)-*block*-polystyrene (denoted P*t*BA-*b*-PS; upper right panel in **Figure 1**) diblock copolymers with precisely controlled molecular weight and low polydispersity of the inner P*t*BA and outer PS blocks were synthesized via sequential ATRP of *tert*-butyl acrylate (*t*BA) and styrene (St) monomers using 21-Br-β-CD as a macroinitiator.[15] Subseqeuently, the inner P*t*BA blocks were hydrolyzed into PAA blocks, resulting in amphiphilic unimolecular star-like PAA-*b*-PS (lower right panel in **Figure 1**). Notably, in contrast to conventional linear block copolymer micelles formed by much weaker forces of attraction, there are 21 arms of PAA-*b*-PS diblock copolymer anchored covalently to a single macroinitiator. Further characterization (e.g. TEM and AFM) of the star-like PAA-*b*-PS diblock copolymer has been previously reported by our group.[16]

Amphiphilic star-like PAA-*b*-PS diblock copolymers were then exploited as nanoreactors to template the synthesis of $CsPbBr_3$ QDs tethered by PS chains that were originally covalently bonded to PAA chains. First, the star-like nanoreactor, cesium bromide (CsBr), and lead bromide ($PbBr_2$) were fully dissolved in N,N-dimethylformamide (DMF). The perovskite ions selectively occupied the inner PAA-containing compartment of the nanoreactor by strongly coordinating with the carboxyl groups of the inner PAA blocks (i.e., forming the CsBr- and $PbBr_2$-loaded nanoreactor solution; lower central panel in **Figure 1**).[11, 13, 15] Subsequently, by dropping the solution into a poor solvent (i.e., toluene) for the perovskite precursors, $CsPbBr_3$ QDs were rapidly produced via co-precipitation[17] in toluene (lower left panel in **Figure 1**), selectively confined within the inner PAA compartment. This is not surprising as perovskite QDs would otherwise be decomposed in DMF due to their ionic nature. It is worth noting that as PS dissolves well in toluene, the aggregation of PS-capped perovskite QDs in toluene was thus prevented.

Synthesis of $CsPbBr_3$ QDs were compared by capitalizing on star-like PAA-*b*-PS nanoreactor (the molecular weight of a single PS chain is 7300 g/mol, thus the resulting QDs are referred to as PS(7k)-capped $CsPbBr_3$ QDs) and by utilizing oleic acid as the common linear ligand, respectively. Oleic acid has been chosen for the control experiment as both PAA and oleic acid have the same functional group (i.e. carboxylic acid) that can bind to perovskite QDs. For the PS(7k)-capped $CsPbBr_3$ QDs, as the precursor solution was dropped

into toluene, co-precipitation of CsBr and $PbBr_2$ occurred selectively within the inner PAA compartment of the star-like PAA-*b*-PS nanoreactor. Due to hydrophobic PS capping, green-emitting QDs rapidly formed in the solution in less than 1 s, suggesting the homogeneous dispersion of QDs in toluene.

In contrast, $CsPbBr_3$ capped with oleic acid and $CsPbBr_3$ with no ligand present were initially bright when the precursor solution was added into toluene; however, the PL of $CsPbBr_3$ quickly disappeared (< 1 s) due to aggregation of QDs. Notably, in contrast to room temperature synthesis via co-precipitation, it has been reported that high-temperature hot-injection of precursors in the presence of oleic acid does produce relatively stable $CsPbBr_3$ QDs,[18] due likely to the temporally discrete nucleation event followed by controlled growth on the existing nuclei achievable at high temperatures.[19] The observations noted above were verified by TEM measurements, where uniform PS(7k)-capped $CsPbBr_3$ QDs with an average size of 13.9±0.7 nm were seen (size distribution within 5% of average size, which can be regarded as monodisperse)**,** while aggregates of $CsPbBr_3$ were found for the oleic acid and no ligand samples. Moreover, HRTEM studies reveal that PS(7k)-capped $CsPbBr_3$ QDs are highly crystalline. In order to further corroborate the formation of $CsPbBr_3$ QDs inside the nanoreactor, star-like PAA-*b*-PS nanoreactors were stained by RuO_4 before and after the formation of $CsPbBr_3$ QDs. Clearly, the ability to craft uniform PS(7k)-capped $CsPbBr_3$ QDs demonstrates the effectiveness of star-like nanoreactor in synthesizing high-quality hairy $CsPbBr_3$ QDs.

Successful synthesis of green-emitting $CsPbBr_3$ QDs was further substantiated by absorption, PL and XRD measurements. It is interesting to note that the FWHM, an indirect measure of the monodispersity of QDs, is as low as 17.7 nm for PS(7k)-capped $CsPbBr_3$ QDs, which is comparable to the lowest value for $CsPbBr_3$ QDs reported,[21] leading to superior color quality for display backlight applications compared to currently used CdSe/ZnS QDs (FWHM ~30nm). Anion exchange of the Br^- group in PS-capped $CsPbBr_3$ QDs using $ZnCl_2$ and ZnI_2 was then performed to yield blue-emitting $CsPbCl_3$ and red-emitting $CsPbI_3$ QDs with their PL peak positions blue-shifted to 427 nm and red-shifted to 700 nm, respectively.[22]

In addition to the composition-dependent tuning of optical properties as noted above, remarkably, the star-like block copolymer nanoreactor strategy can also effectively alter the size of QDs to manipulate their optical properties. By synthesizing the star-like diblock copolymer with precisely controlled length (i.e., molecular weight) of each block and low polydispersity via ATRP, the size of QDs can be accurately regulated (**Figure 2a**), thereby rendering strict control over light harvesting and emission of QDs at desired wavelengths in the visible region (**Figure 2b**). The size of the three PS-capped $CsPbBr_3$ QDs crafted are 8.6±0.3 nm, 10.1±0.6 nm, 13.9±0.7 nm, and their corresponding PL peaks are at 514 nm, 515 nm, and 516 nm, respectively. It is notable that as the sizes of these crafted QDs are above the Bohr diameter of $CsPbBr_3$ of 7 nm,[1] the PL peak position change is minimal. In contrast, for PS-capped $CsPb(Br_{0.1}I_{0.9})_3$ synthesized by partial anion exchange of $CsPbBr_3$ with ZnI_2 which has a Bohr diameter of nearly 12 nm,[1] the PL peak positions are more distinctly apart at 685 nm, 695 nm, and 698 nm, respectively, clearly displaying the quantum confinement effect (**Figure 2b**). As PL trends show, further reduction in the nanoreactor dimension (i.e. smaller PAA block molecular weight) will continue to reduce QD dimensions leading to further blue-shift in PL. All PS-capped $CsPbBr_3$ QDs (D = 13.9 nm, 10.1 nm, and 8.6 nm) are crystalline as revealed by HRTEM (lower panels in **Figure 2a**). The green-emitting PS-capped $CsPbBr_3$ QDs (D = 13.9 nm) exhibited a high QY of 91.4% and a FWHM as low

as 17.7 nm. As the size of the PS-capped $CsPbBr_3$ QDs decreased, the QY decreased to 84.9% (D = 10.1 nm) and 67% (D = 8.6 nm), which may be due to the higher weight fraction of PAA groups in smaller PS-capped $CsPbBr_3$ QDs and large surface-to-volume ratio of smaller-sized QDs that may possess higher density of surface defects.[23] It is important to note that in order to minimize the effect from the surface defects, post-treatment via zinc bromide was conducted to passivate the PS-capped $CsPbBr_3$ QD surface.[24] Thus, it is highly likely that the reduction in QY is due to the PAA inside the QD. It is also noteworthy that, however, the reduction in QY due to the PAA is substantially reduced as the size of the QD is increased as seen from the excellent QY (91%) of the 13.9-nm PS-capped $CsPbBr_3$ QDs. Moreover, it should be noted that despite the existence of PAA chains within $CsPbBr_3$ QDs and the lack of inorganic shell as in core/shell QDs to reduce surface defects, the high QY observed in $CsPbBr_3$ QDs is due largely to the high defect-tolerance characteristic of perovskite material as a result of unique band structure and optical properties.[25] The valence band maximum (VBM) of perovskite is antibonding in nature and the conduction band minimum is stabilized by strong spin−orbit coupling, as opposed to common II−VI and III−V QDs wherein VBM is constituted by bonding orbitals. To further evaluate the effect star-like nanoreactors have on the $CsPbBr_3$ QDs, the characteristic time-resolved PL (TRPL) decay lifetime as a function of QD size was also measured. From the QY and TRPL measurements, the radiative and non-radiative decay rates of the PS-capped $CsPbBr_3$ QDs were calculated. For PS-capped $CsPbBr_3$ QDs after complete surface passivation with zinc bromide, the non-radiative decay rate shows a steady decrease (i.e., 5 us^{-1} at D = 8.6 nm, 2.6 us^{-1} at D = 10.1 nm, and 1.9 us^{-1} at D = 13.9 nm) as the QD size increases, which agrees well with higher QY values observed for larger QDs. The TRPL decay curves were best-fit using a biexponential decay function:

$$A(t) = A_1 exp\left(-\frac{t}{\tau_1}\right) + A_2 exp\left(-\frac{t}{\tau_2}\right)$$

where A, A_1, and A_2 are constants; t is time; τ_1 and τ_2 are PL decay lifetimes.[27, 31] For better comparison between each sample, the average PL decay lifetime, τ_{avg}, radiative decay rate, k_{rad}, and non-radiative decay rate, $k_{non-rad}$ were calculated using the following equations:

$$\tau_{avg} = \frac{A_1\tau_1^2 + A_2\tau_2^2}{A_1\tau_1 + A_2\tau_2} = \frac{1}{k_{rad} + k_{non-rad}} \quad (1)$$

$$\text{QY} = \frac{k_{rad}}{k_{rad} + k_{non-rad}} \quad (2)$$

$$k_{rad} = \frac{PLQY}{\tau_{avg}} \quad (3)$$

$$k_{non-rad} = \frac{1 - PLQY}{\tau_{avg}} \quad (4)$$

It is interesting to note that the lifetime increases as the QD size decreases (i.e., 66.3 ns at D = 8.6 nm, 58.4 ns at D = 10.1 nm, and 46.4 ns at D = 13.9 nm), suggesting that the PAA chains inside the QD may have the effect on delaying the PL decay. The fact that PL lifetimes for conventional ligand-capped $CsPbBr_3$ QDs are shorter (< 25 ns)[17, 21, 24, 26, 27] than all of the PS-capped $CsPbBr_3$ QDs further corroborates the effect of the presence of PAA chains on increasing PL lifetime. Nonetheless, this merits a detailed study and will be performed by systematically varying the number of PAA arms (i.e., the volume fraction of PAA) while maintaining the QD size in the near future.

Intriguingly, by increasing the molecular weight (i.e., chain length) of PS blocks, the

water stability of PS-capped QDs increased by 33% from 36.3±5.7 min for PS(7k)-capped $CsPbBr_3$ QDs (D = 13.9 nm) to 48.3±0.6 min for PS(16k)-capped $CsPbBr_3$ QDs (D = 13.9 nm). More interestingly, by decreasing the QD size from 13.9 nm to 8.6 nm while keeping the PS length constant, the water stability increased by 28%, that is, from 48.3±0.6 min for PS(16k)-capped $CsPbBr_3$ QDs (D = 13.9 nm) to 61.7±3.2 min for PS(16k)-capped $CsPbBr_3$ QDs (D = 8.6 nm). Remarkably, in stark contrast to $CsPbBr_3$ QDs synthesized via conventional ligand-assisted co-precipitation methods either capped by oleic acid (2.8±0.3 min) or co-capped by oleic acid and oleylamine (5.0±0.5 min), the water stability of PS-capped $CsPbBr_3$ QDs was up to 20 times longer. We note that all experiments were performed under vigorous stirring (1500 rpm) that greatly accelerated the degradation process compared to those in literature. Moreover, our data displayed the stability improvement while forming individual nanoscale coating around each QD; this contrasts to the simple mixing of perovskite QDs in macroscale polymer matrices in literature. To further test water stability, a drop of the PS(7k)-capped $CsPbBr_3$ QDs (D = 13.9 nm) as well as oleic acid & oleyl amine-co-capped $CsPbBr_3$ QDs were dried on a glass substrate and then directly placed in water. PS-capped $CsPbBr_3$ QDs exhibited nearly no loss in PL for 4 h, while the oleic acid & oleyl amine-co-capped $CsPbBr_3$ QDs showed a drastic decay even after 10 min.

It is not surprising that PS-capped $CsPbBr_3$ QDs also exhibited superior colloidal stability when stored in toluene. The permanently ligated PS chains on the perovskite QD surface are well dissolved in good solvent, toluene, leading to excellent dispersion of PS-capped $CsPbBr_3$ QDs without aggregation. The QY of PS-capped $CsPbBr_3$ QDs toluene solution was maintained for more than 535 days without any decrease. It is also notable that there was no significant shift in the PL peak position as well as the FWHM, signifying minimal or no change in the size distribution of QDs over the 535-day period. In sharp contrast, oleic acid-capped $CsPbBr_3$ QDs displayed a PL peak shoulder and a 22% increase in PL FWHM only after 24 h storage under ambient conditions.

The markedly improved colloidal and water stabilities of PS-capped QDs can be rationalized as follows. As toluene is a good solvent for PS, the intimately and permanently tethered PS chains on the perovskite QD surface are fully extended as a result of favorable interaction between toluene and PS, yielding excellent colloidal stability. However, when water is introduced, the hydrophobic PS chains collapse onto the perovskite QD due to the poor solubility of PS in water. The collapsed PS chain forms a PS shell surrounding the perovskite QD surface, thereby preventing water from reaching and degrading the perovskite QD due to its ionic nature (**Figure 3b-d**). It is worth noting that longer PS chains (16k PS (**Figure 3c**) compared to 7k PS (**Figure 3b**)) impart denser hydrophobic PS shell situated on the perovskite QD surface and thus further effectively blocks water penetration through the shell, leading to enhanced stability against water. As the size of QDs capped with the same length of PS chains decreases (13.9-nm compared to 8.6-nm $CsPbBr_3$ QDs capped by 16k PS chains), the surface of QD is further adequately covered by PS, resulting in progressively improved water stability (**Figure 3d**). Clearly, each PS-capped $CsPbBr_3$ QD, for the first time, possesses a separate protective shell that can be precisely tailored to any desired length (or thickness when in contact with water). In contrast to PS-capped $CsPbBr_3$ QDs, due to the weak coordination bonding between small-molecule ligands (e.g., oleic acid & oleylamine) and QDs, these ligands collapsed on the $CsPbBr_3$ QD surface upon the addition of water would dissociate from the QD surface. Consequently, water contacts the exposed surface of QDs, causing their decomposition into precursors and the diminishing of fluorescence (**Figure 3a**).

Due to their high QY, narrow FWHM, size- and composition-dependent emission tunability, and solution processability, perovskite QDs represent next-generation materials for use in display and solid-state lighting. In this context, as as-synthesized PS-capped perovskite QDs show good optical properties, their potential application in WLED was demonstrated (**Figure 4**). **Figure 4a** presents the PL spectra of the WLED device with three distinct peaks from the GaN blue-chip (blue), PS-capped $CsPbBr_3$ QDs (green), and $CdSe/Cd_{1-x}Zn_xSe_{1-y}S_y/ZnS$ QDs (red), respectively. A digital image of an actual WLED device emitting white light is shown as an inset. **Figure 4b** displays the Commission Internationale de L'Eclairage (CIE) diagram. The WLED prototype containing the PS-capped $CsPbBr_3$ QDs has a color coordinate of (0.31, 0.32), very close to the white color coordinate of (0.33, 0.33). The color gamut of PS-capped $CsPbBr_3$ QD-based WLED is 130% over that of NTSC and 184% over that of sRGB standards. To verify the improved stability of PS-capped $CsPbBr_3$ QDs in the PMMA matrix used in LEDs, a thermal cycling stability experiment was performed between 25°C to 100°C. The results show a 96% retention in original PL for PS-capped $CsPbBr_3$ QDs in the PMMA matrix compared to a retention of only 45% in oleic acid & oleyl amine-co-capped $CsPbBr_3$ QDs.

Conclusion

In summary, we demonstrated the precision synthesis of perovskite QDs with varied sizes and compositions permanently anchored by hydrophobic polymer chains via capitalizing on judiciously designed amphiphilic star-like diblock copolymers as nanoreactors. Due to living free radical polymerization characteristic, ATRP entails the synthesis of star-like diblock copolymer with well-controlled molecular weight and low PDI of each block. Consequently, the size of PS-capped $CsPbX_3$ QDs, formed via strong coordination interaction of perovskite precursors with the inner hydrophilic PAA blocks of star-like PAA-*b*-PS, can be precisely tailored, thereby offering delicate control over absorption and emission of $CsPbX_3$ QDs. Green-emitting PS-capped $CsPbBr_3$ QDs crafted exhibit high QY of 91% after surface passivation with zinc bromide and low FWHM of 17.7 nm. Notably, subsequent anion exchange of the halide group renders a series of effective tuning of emission of PS-capped QDs from 427 nm (blue) to 700 nm (red). It is important to note that each PS-capped $CsPbX_3$ QD, for the first time, carries a layer of protective hydrophobic PS chains that can be readily regulated to any desired length during the ATRP of St monomers. Such permanently ligated length-tunable PS shell on the $CsPbX_3$ surface affords strikingly improved water and colloidal stabilities in harsh environment (e.g., deliberately added water) that is often not experienced under regular operating condition. When directly exposed to water, the PS chains collapse onto the perovskite QD due to its poor solubility in water, forming a dense PS cushion on the perovskite QD surface and thus greatly preventing water from reaching and dissolving the perovskite QD. In striking contrast to $CsPbBr_3$ QDs synthesized via conventional ligand-assisted approaches, PS-capped $CsPbBr_3$ QDs impart a twentyfold improvement in water stability. In addition, PS-capped $CsPbBr_3$ QDs also manifest superior colloidal stability which can be attributed to the fact that the perovskite QDs are intimately and stably ligated by PS chains that are fully extended in good solvent toluene. As a result, PS-capped $CsPbBr_3$ QDs demonstrate excellent colloidal stability for more than 535 days with no change in QY, PL wavelength, and FWHM. WLED constructed using hairy perovskite QDs demonstrates 130% and 184% color gamut over NTSC and sRGB standards, respectively. Finally, as star-like nanoreactor strategy is amenable for the synthesis of a large array of hairy polymer-capped nanocrystals, uniform perovskite QDs with controlled dimensions, desired functionality (e.g., environmentally benign, lead-free $CsSbBr_3$ QDs using star-like PAA-*b*-PE as nanoreactor; organic-inorganic hybrid perovskite QDs such as

$CH_3NH_3PbI_3$; etc.), design complexity (e.g., hairy core/shell perovskite QDs via star-like triblock copolymer nanoreactors), and high stability can be readily crafted.

References

[1] G. Nedelcu, L. Protesescu, S. Yakunin, M. Bodnarchuk, M. Grotevent, M. Kovalenko, *Nano Lett.* **2015**, 15, 5635.

[2] X. Zhang, H. Lin, H. Huang, C. Reckmeier, Y. Zhang, W. Choy, A. Rogach, *Nano Lett.* **2016**, 16, 1415.

[3] M. Cha, P. Da, J. Wang, W. Wang, Z. Chen, F. Xiu, G. Zheng, Z. Wang, *J. Am. Chem. Soc.* **2016**, 138, 8581.

[4] L. Protesescu, S. Yakunin, M. I. Bodnarchuk, F. Krieg, R. Caputo, C. H. Hendon, R. X. Yang, A. Walsh, M. V. Kovalenko, *Nano Lett.* **2015**, 15, 3692.

[5] H. Zhu, Y. Fu, F. Meng, X. Wu, Z. Gong, Q. Ding, M. Gustafsson, M. Trinh, S. Jin, X. Zhu, *Nat. Mater.* **2015**, 14, 636.

[6] J. Song, J. Li, X. Li, L. Xu, Y. Dong, H. Zeng, *Adv. Mater.* **2015**, 27, 7162.

[7] H.-C. Wang, S.-Y. Lin, A.-C. Tang, B. P. Singh, H.-C. Tong, C.-Y. Chen, Y.-C. Lee, T.-L. Tsai, R.-S. Liu, *Angew. Chem. Int. Ed.* **2016**, 55, 7924.

[8] Q. A. Akkerman, V. D'Innocenzo, S. Accornero, A. Scarpellini, A. Petrozza, M. Prato, L. Manna, *J. Am. Chem. Soc.* **2015**, 137, 10276.

[9] C. Wang, Y. Zhang, A. Wang, Q. Wang, H. Tang, W. Shen, Z. Li, Z. Deng, *Chem. Mater.* **2017**, 29, 2157.

[10] A. Loiudice, S. Saris, E. Oveisi, D. T. L. Alexander, R. Buonsanti, *Angew. Chem. Int. Ed.* **2017**, 56, 10696.

[11] Y. Chen, Z. Wang, Y. He, Y. J. Yoon, J. Jung, G. Zhang, Z. Lin, *PNAS* **2018**, 115, E1391.

[12] H. Zhang, X. Wang, Q. Liao, Z. Xu, H. Li, L. Zheng, H. Fu, *Adv. Funct. Mater.* **2017**, 27, 1604382; S. N. Raja, Y. Bekenstein, M. A. Koc, S. Fischer, D. Zhang, L. Lin, R. O. Ritchie, P. Yang, A. P. Alivisatos, *ACS Appl. Mater. Interfaces* **2016**, 8, 35523.

[13] Y. Chen, D. Yang, Y. J. Yoon, X. Pang, Z. Wang, J. Jung, Y. He, Y. W. Harn, M. He, S. Zhang, G. Zhang, Z. Lin, *J. Am. Chem. Soc.* **2017**, 139, 12956.

[14] M. Massignani, C. LoPresti, A. Blanazs, J. Madsen, S. P. Armes, A. L. Lewis, G. Battaglia, *Small* **2009**, 5, 2424.

[15] X. Pang, L. Zhao, W. Han, X. Xin, Z. Lin, *Nat. Nanotech.* **2013**, 8, 426.

[16] X. Pang, L. Zhao, M. Akinc, J. K. Kim, Z. Lin, *Macromolecules* **2011**, 44, 3746.

[17] X. Li, Y. Wu, S. Zhang, B. Cai, Y. Gu, J. Song, H. Zeng, *Adv. Funct. Mater.* **2016**, 26, 2435.

[18] E. Yassitepe, Z. Yang, O. Voznyy, Y. Kim, G. Walters, J. A. Castañeda, P. Kanjanaboos, M. Yuan, X. Gong, F. Fan, J. Pan, S. Hoogland, R. Comin, O. M. Bakr, L. A. Padilha, A. F. Nogueira, E. H. Sargent, *Adv. Funct. Mater.* **2016**, 26, 8757.

[19] C. B. Murray, D. J. Norris, M. G. Bawendi, *J. Am. Chem. Soc.* **1993**, 115, 8706.

[20] Y. Chen, Y. J. Yoon, X. Pang, Y. He, J. Jung, C. Feng, G. Zhang, Z. Lin, *Small* **2016**, 12, 6714.

[21] F. Krieg, S. T. Ochsenbein, S. Yakunin, S. ten Brinck, P. Aellen, A. Süess, B. Clerc, D. Guggisberg, O. Nazarenko, Y. Shynkarenko, S. Kumar, C.-J. Shih, I. Infante, M. V. Kovalenko, *ACS Energy Lett.* **2018**, 3, 641.

[22] T. Zhang, G. Li, Y. Chang, X. Wang, B. Zhang, H. Mou, Y. Jiang, *CrystEngComm* **2017**, 19, 1165.

[23] J. Kang, L.-W. Wang, *J. Phys. Chem. Lett.* **2017**, 8, 489.

[24] F. Li, Y. Liu, H. Wang, Q. Zhan, Q. Liu, Z. Xia, *Chem. Mater.* **2018**, 30, 8546.

[25] A. Swarnkar, V. K. Ravi, A. Nag, *ACS Energy Lett.* **2017**, 2, 1089.

[26] W. van der Stam, J. J. Geuchies, T. Altantzis, K. H. W. van den Bos, J. D. Meeldijk, S. Van Aert, S. Bals, D. Vanmaekelbergh, C. de Mello Donega, *J. Am. Chem. Soc.* **2017**, 139, 4087.

[27] A. Shinde, R. Gahlaut, S. Mahamuni, *J. Phys. Chem. C* **2017**, 121, 14872.

[28] X. Pang, L. Zhao, C. Feng, Z. Lin, *Macromolecules* **2011**, 44, 7176.

[29] Y. Chang, Y. J. Yoon, G. Li, E. Xu, S. Yu, C.-H. Lu, Z. Wang, Y. He, C. H. Lin, B. K. Wagner, V. V. Tsukruk, Z. Kang, N. Thadhani, Y. Jiang, Z. Lin, *ACS Appl. Mater. Interfaces* **2018**, 10, 37267.

[30] J. Jung, C. H. Lin, Y. J. Yoon, S. T. Malak, Y. Zhai, E. L. Thomas, V. Vardeny, V. V. Tsukruk, Z. Lin, *Angew. Chem. Int. Ed.* **2016**, 55, 5071.

[31] C. Liu, Z. Li, T. J. Hajagos, D. Kishpaugh, D. Y. Chen, Q. Pei, *ACS Nano* **2017**, 11, 6422.

Figures and Figure Captions

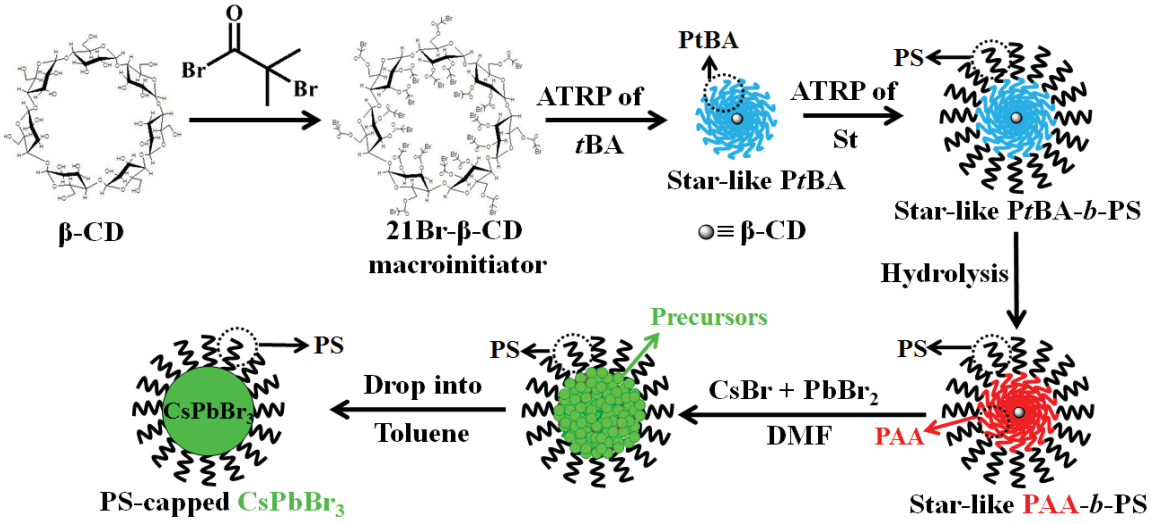

Figure 1. Stepwise representation of crafting hairy all-inorganic perovskite $CsPbBr_3$ QDs intimately and permanetnly capped by PS chains via capitalizing on amphiphilic star-like PAA-*b*-PS diblock copolymer as nanoreactor.

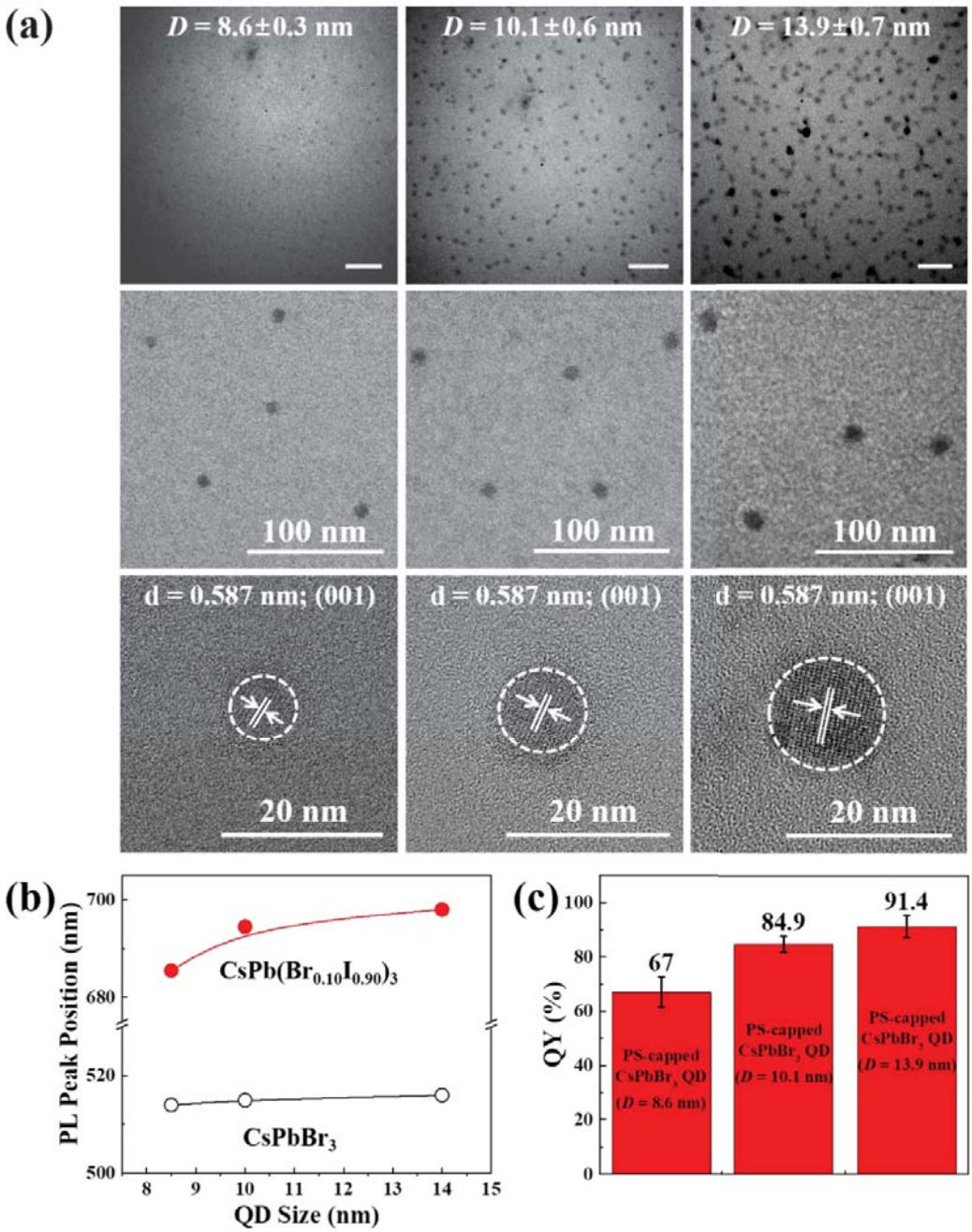

Figure 2. Size-dependent optical properties of PS-capped $CsPbX_3$ QDs. (a) TEM images of PS-capped $CsPbBr_3$ QDs of three different sizes. Column 1: D=8.6±0.3 nm; crafted using sample 1 in **Table S2**). Column 2: D=10.1±0.6 nm, crafted using sample 3 in **Table S2**. Column 3: D=13.9±0.7 nm; crafted using sample 5 in **Table S2.** The corresponding HRTEM images are shown in the last row, where the (001) plane has a lattice spacing d=0.587 nm. (b) Effect of QD size on the PL peak position. Open circle: PS-capped $CsPbBr_3$ QDs. Solid circle: PS-capped $CsPb(Br_{0.1}I_{0.9})_3$ QDs. (c) Quantum yields (QYs) of PS-capped $CsPbBr_3$ QDs of different sizes.

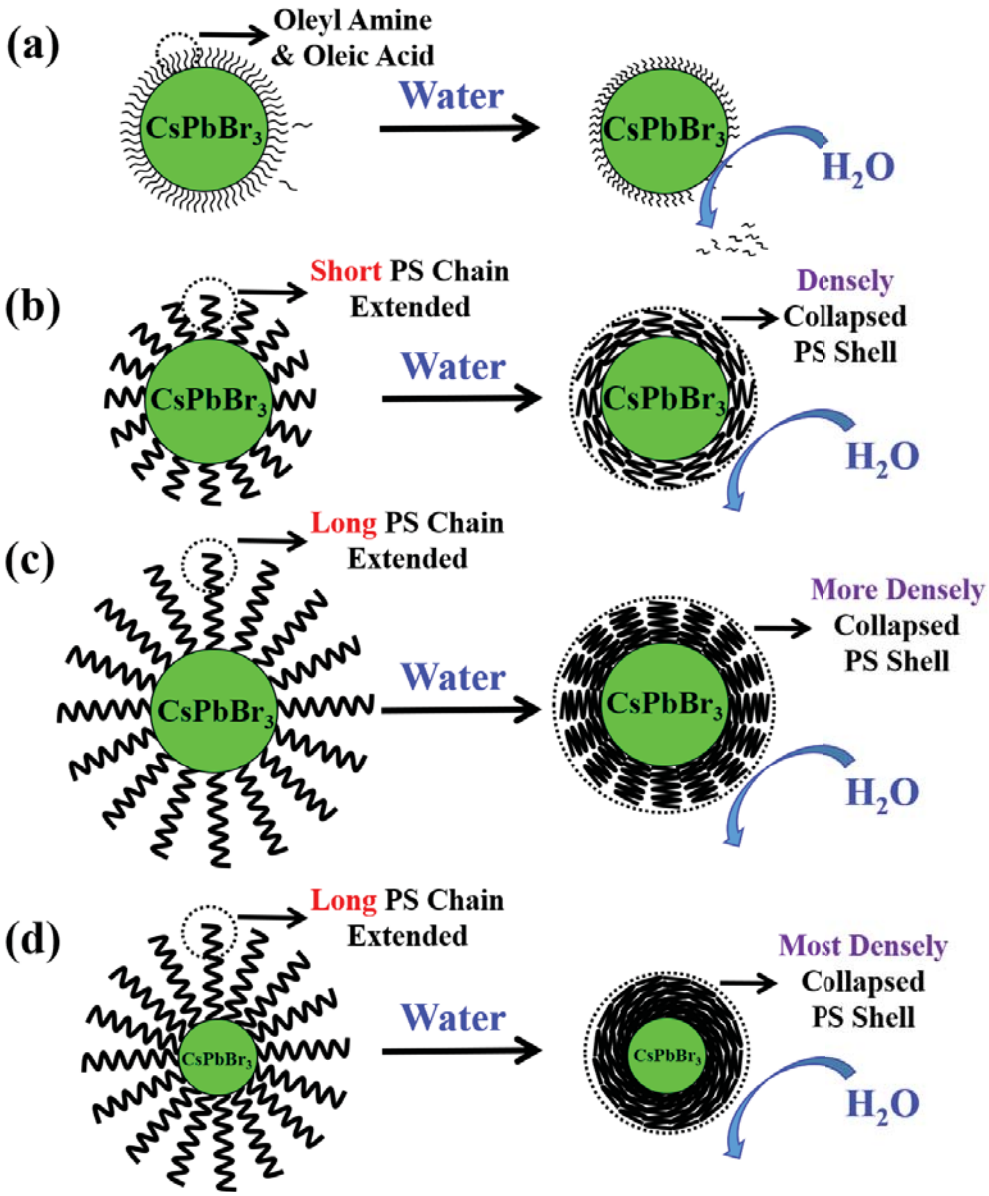

Figure 3. Illustration of PS-capped QDs with varied QD sizes and length of PS chains for markedly improved colloidal and water stabilities. (a) Ligand loss from the perovskite QD surface upon water exposure in oleylamine/oleic acid co-capped $CsPbBr_3$ QDs. (b-d) PS chains collapse onto the perovskite QD surface upon water exposure. (b) Permanently-grafted PS(7k) forms a PS shell layer around $CsPbBr_3$ QD (D=13.9 nm; PS(7k)-capped $CsPbBr_3$ QDs synthesized using sample 5 in **Table S2**). (c) Permanently-tethered PS(16k) forms a denser PS shell layer on the surface of $CsPbBr_3$ QD (D=13.9 nm; PS(16k)-capped $CsPbBr_3$ QDs crafted using sample 6 in **Table S2**). (d) Permanently-capped PS(16k) forms an even denser PS shell layer situated on smaller-sized $CsPbBr_3$ QDs (D=8.6 nm; PS(16k)-capped $CsPbBr_3$ QDs yielded using sample 2 in **Table S2**).

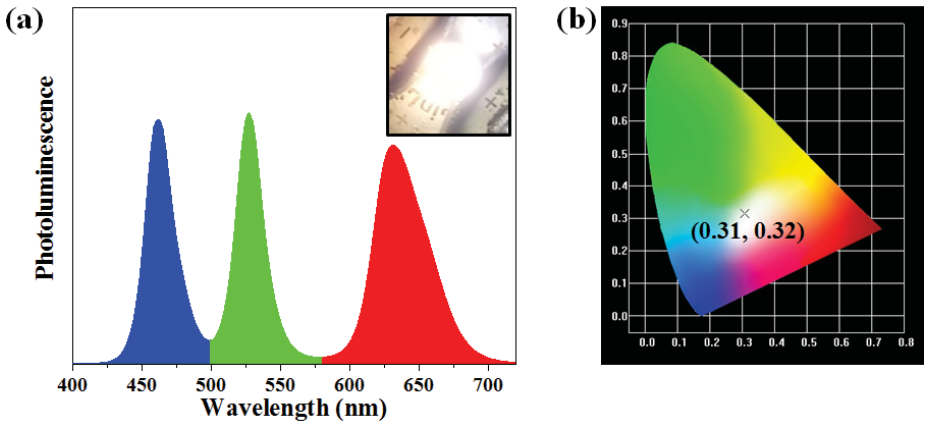

Figure 4. PS-capped $CsPbBr_3$ QD-based white light emitting diode (WLED). (a) PL spectra of PS-capped $CsPbBr_3$ QD-based WLED device. Inset shows a digital image of WLED device. (b) CIE color diagram of the WLED device.

Publications from 05/2018 to 04/2019 on this AFOSR project (11 papers total)

1. Y. Chen, Z. Wang, Y. W. Harn, S. Pan, Z. Li, S. Lin, J. Peng, G. Zhang, and **Z. Lin***, "Resolving Paradox on Optical and Catalytic Activities in Thermoresponsive Nanoparticles via Permanent Ligating with Temperature-Sensitive Polymers", ***Science Advances*** (submitted)

2. Y. J. Yoon, Y. Chang, S. Zhang, S. Pan, Y. He, C. Lin, S. Yu, Y. Chen, Z. Wang, J. Jung, N. Thadhani, V. Tsukruk, Z. Kang, and **Z. Lin*,** "Enabling Tailorable Optical Properties and Markedly Enhanced Stability of Perovskite Quantum Dots by Permanently Ligating with Polymer Hairs", ***Advanced Materials*** (revised manuscript submitted)

3. B. Jiang, J. Iocozzia, L. Zhao, H. Zhang,Y.-W. Harn, Y. Chen, and **Z. Lin***, "Barium Titanate at the Nanoscale: Controlled Synthesis and Dielectric and Ferroelectric Properties", ***Chemical Society Reviews***, **48**, 1194 (2019).

4. (247) E. Lafalce, Q. Zeng, C. H. Lin, M. Smith, S. Malak, J. Jung, Y. Yoon, **Z. Lin**, V. V. Tsukruk, Z. V. Vardeny, "Robust lasing modes in colloidal quantum dot microdisks using a non-Hermitian exceptional point", ***Nature Communications*** 10, 561 (2019)

5. Y. Chen, Z. Wang, Y. He, Y. J. Yoon, J. Jung, G. Zhang*, and **Z. Lin***, "Light-Enabled Reversible Self-Assembly and Tunable Optical Properties of Stable Hairy Nanoparticles", ***Proceedings of the National Academy of Sciences of the United State of America***, **115**, E1391 (2018).

6. X. Li, J. Iocozzia, Y. Chen, S. Zhao, X. Cui, W. Wang, H. Yu, S. Lin, and **Z. Lin***, "From Precision Synthesis of Block Copolymers to Properties and Applications of Nanoparticles", ***Angewandte Chemie International Edition***, **57**, 2046 (2018).

7. X. Li, B. Li, M. He, W. Wang, T. Wang, A. Wang, J. Yu, Z.L. Wang, S. W. Hong, M. Byun, S. Lin, H. Yu, and **Z. Lin***, "Convenient and Robust Route to Photoswitchable Hierarchical Liquid Crystal Polymer Stripes via Flow-Enabled Self-Assembly", ***ACS Applied Materials & Interfaces***, **10**, 4961(2018).

8. X. Meng, X. Cui, M. Rager, S. Zhang, Z. Wang, J. Yu, Y. Harn, Z. Kang, B. K. Wagner, Y. Liu, C. Yu, J. Qiu,* and **Z. Lin***, "Cascade charge transfer enabled by incorporating edge-enriched graphene nanoribbons for mesostructured perovskite solar cells with enhanced performance", ***Nano Energy***, **52**, 123 (2018).

9. Y. Chang, Y. Yoon, G. Li, E. Xu, S. Yu, C. Lu, Z. Wang, Y. He, C. Lin, B. K. Wagner, V. V. Tsukruk, Z. Kang, N. Thadhani, Y. Jiang*, and **Z. Lin***, "All-Inorganic Perovskite Nanocrystals with a Stellar Set of Stabilities and Their Use in White Light-Emitting Diodes", ***ACS Applied Materials & Interfaces***, **10**, 37267 (2018).

10. D. Yang, Y. Chen, H. Peng, G. Chen, and **Z. Lin***, "An integrated experimental and theoretical study on optical properties of uniform hairy noble metal nanoparticles", ***Nanoscale***, **10**, 22750 (2018).

11. C. Lin, Q. Zeng, E. Lafalce, S. Yu, M. J. Smith, Y. Yoon, Y. Chang, Y. Jiang, **Z. Lin**, Z. V. Vardeny, and V. V. Tsukruk, "Large-Area Lasing and Multicolor Perovskite Quantum Dot Patterns", ***Advanced Optical Materials***, **6**, 1800474 (2018).